



# VCU

Virginia Commonwealth University  
VCU Scholars Compass

---

Theses and Dissertations

Graduate School

---

2018

## The Role Of A Type Lamins In Regulating Myelination

Jacqueline M. DeLoyht  
*Virginia Commonwealth University*

Follow this and additional works at: <https://scholarscompass.vcu.edu/etd>



Part of the [Nervous System Commons](#)

© The Author

---

Downloaded from

<https://scholarscompass.vcu.edu/etd/5388>

This Thesis is brought to you for free and open access by the Graduate School at VCU Scholars Compass. It has been accepted for inclusion in Theses and Dissertations by an authorized administrator of VCU Scholars Compass. For more information, please contact [libcompass@vcu.edu](mailto:libcompass@vcu.edu).

# THE ROLE OF A TYPE LAMINS IN REGULATING MYELINATION

A thesis submitted in partial fulfillment of the requirements for the degree of Master of Science  
at Virginia Commonwealth University.

by

JACQUELINE MICHELLE DELOYHT

Bachelor of Science in Biology, Virginia Commonwealth University, 2011

Director: DR. JEFFREY L. DUPREE, PhD

ASSISTANT PROFESSOR, ANATOMY AND NEUROBIOLOGY

Virginia Commonwealth University

Richmond, Virginia

April, 2018

## ACKNOWLEDGEMENTS

I would first like to express my gratitude to my advisor, Dr. Dupree, for his immeasurable help throughout not only my graduate studies, but my entire experience in basic science research. He has been an outstanding mentor from the first day I stepped into his laboratory as an undergraduate. He has been a source of wisdom, encouragement, endless patience, and invaluable guidance.

I would like to thank my committee members Dr. Sato-Bigbee and Dr. Devries for their input and advice, as well as their compassionate and encouraging approach to graduate students.

Thank you to Dr. Casaccia, without whom, this investigation would not be possible. The ability to be part of a collaboration with her laboratory has been an honor and privilege.

I would like to thank Dr. Colello and Dr. Bigbee for the opportunity to pursue my graduate studies. Additionally, thank you to Mr. Greenwald for his immense help navigating the details of the graduate program, and handling it all with kindness and a sense of humor.

Lastly, I express my sincerest gratitude to my family for being a source of unending support and faith in my capabilities. To my mother, who never stopped believing in me, and supported me unconditionally. To her, and in memorial of my father, I dedicate this thesis.

**TABLE OF CONTENTS**

	Page
Acknowledgements.....	ii
List of Figures.....	vii
Abbreviations.....	ix
Abstract.....	xi
Introduction.....	1
Multiple Sclerosis.....	2
Current Multiple Sclerosis treatments.....	3
The Neuron.....	4
Oligodendrocytes.....	7
Oligodendrocyte Differentiation.....	7
Myelin.....	11
CNS Myelin.....	11
Myelination in the Murine CNS.....	12
Chromatin and Gene Expression.....	13
Nuclear Lamina.....	17
Lamins.....	17

B type lamins.....	21
A type lamins.....	21
<i>LMNA</i> Null Mutant.....	22
Project aim.....	23
Materials and Methods.....	25
Animals.....	25
Perfusion.....	25
Electron microscopy tissue processing.....	26
Image Collection Using Transmission Electron Microscopy.....	28
Heterochromatin analysis.....	29
G-ratio analysis.....	43
Measurement of Nucleus : Cytoplasm Ratio.....	43
Results.....	45
No difference was observed in heterochromatin ratios or distribution in the oligodendrocyte nucleus of PND 21 WT and <i>LMNA</i> KO mice.....	45
Heterochromatin distribution in the corpus callosum of PND 21 mice.....	45

Heterochromatin distribution in the spinal cord of PND 21 mice.....	46
Mean myelin thickness did not differ between WT and <i>LMNA</i> KO at PND 21 in either the corpus callosum or spinal cord.....	47
No difference in ratios of oligodendrocyte nuclear area to cytoplasm area was observed between WT and <i>LMNA</i> KO at PND 21.....	48
<i>LMNA</i> plays a role in heterochromatin organization in PND 35 mice.....	48
<i>LMNA</i> regulates heterochromatin organization in corpus callosum oligodendrocytes of PND 35 mice.....	49
No difference in heterochromatin distribution in the optic nerve of PND 35 <i>LMNA</i> KO mice.....	50
<i>LMNA</i> plays a role in heterochromatin organization in spinal cord oligodendrocytes of PND 35 mice.....	50
Myelin thickness is reduced in the absence of <i>LMNA</i> in a region specific manner at PND 35.....	51
Absence of <i>LMNA</i> does not have an effect on myelin thickness in the corpus callosum of PND 35 mice.....	52
<i>LMNA</i> impacts myelin thickness in the spinal cord of PND 35 mice.....	52
Ratios of oligodendrocyte nuclear area to cytoplasm area are not altered in the absence of <i>LMNA</i> in PND 35 mice.....	53
Results summary.....	53
Discussion.....	85
<i>LMNA</i> affects heterochromatin architecture in the oligodendrocyte nucleus temporally and spatially.....	86
<i>LMNA</i> plays a temporal role in spinal cord myelination.....	88
<i>LMNA</i> does not impact oligodendrocyte maturity.....	89

Future directions.....	90
Concluding remarks.....	91
Literature Cited.....	92
Vita.....	104

## LIST OF FIGURES

1.1. CNS Myelinated Neuron Schematic.....	6
1.2. Oligodendrocyte Development.....	10
1.3. Chromatin Structure.....	16
1.4. Lamins and the Nuclear Envelope.....	20
2.1. Selection of oligodendrocyte nuclear area.....	32
2.2. Isolation of oligodendrocyte nuclear area.....	34
2.3. Selection and elimination of nucleolus from analysis.....	36
2.4. Thresholding and selection of heterochromatin.....	38
2.5. Peripheral heterochromatin selection.....	40
2.6. Peripheral heterochromatin isolation and thresholding.....	42
3.1. PND 21 Corpus callosum oligodendrocytes show no difference in heterochromatin distribution.....	56
3.2. PND 21 Spinal cord oligodendrocytes show no difference in heterochromatin distribution.....	58
3.3. No difference in heterochromatin of PND 21 spinal cord ventral horn motor neurons.....	60
3.4. G ratios of myelinated axons were not different in the corpus callosum at PND 21.....	62
3.5. PND 21 spinal cord myelinated axons show no difference in myelin thickness.....	64
3.6. Oligodendrocytes from the spinal cord or corpus callosum from WT and <i>LMNA</i> KO mice revealed no difference in nucleus to cytoplasm ratio in PND 21 mice.....	66

3.7. Peripheral Heterochromatin was significantly reduced in the oligodendrocytes from the corpus callosum of PND 35 <i>LMNA</i> KO compared to WT mice.....	68
3.8. PND 35 cortical neurons display no difference in heterochromatin distribution.....	70
3.9. PND 35 optic nerve oligodendrocytes show no difference in heterochromatin distribution..	72
3.10. No difference in heterochromatin of PND 35 optic nerve astrocytes.....	74
3.11. Heterochromatin organization is altered in the spinal cord of PND 35 <i>LMNA</i> KO mice....	76
3.12. PND 35 spinal cord neurons show no difference in heterochromatin distribution.....	78
3.13. G ratios of myelinated axons were not different between genotypes in the corpus callosum at PND 35.....	80
3.14. G ratios of spinal cord myelinated axons were significantly thinner in the <i>LMNA</i> KO mice compared to the WT animals at PND 35.....	82
3.15. Oligodendrocytes from the optic nerve, spinal cord or corpus callosum from WT and <i>LMNA</i> KO revealed no difference in nucleus to cytoplasm ratio at PND 35.....	84

## ABBREVIATIONS

ADLD.....	Autosomal Dominant Leukodystrophy
CNP.....	2':3'-Cyclic Nucleotide 3'-Phosphodiesterase
CNS.....	Central Nervous System
DMT.....	Disease Modifying Treatments
ER.....	Estrogen Receptor
GFAP.....	Glial Fibrillary Acidic Protein
H3K9.....	Histone 3 Lysine 9
HDAC.....	Histone Deacetylase
KO.....	Knockout
LAD.....	Lamina Associated Domains
MAG.....	Myelin Associate Glycoprotein
MBP.....	Myelin Basic Protein
MS.....	Multiple Sclerosis
NAWM.....	Normal Appearing White Matter
NSC.....	Neural Stem Cells
OPC.....	Oligodendroglial Progenitor Cells

PLP.....Proteolipid Protein

PND.....Postnatal Day

PNS.....Peripheral Nervous System

PPMS.....Primary Progressive Multiple Sclerosis

RRMS.....Relapsing Remitting Multiple Sclerosis

SPMS.....Secondary Progressive Multiple Sclerosis

SVZ.....Subventricular Zone

TEM.....Transmission Electron Microscopy

WT.....Wild Type

## ABSTRACT

### THE ROLE OF A TYPE LAMINS IN REGULATING MYELINATION

By Jacqueline M. DeLoyht

A thesis submitted in partial fulfillment of the requirements for the degree of Master of Science at Virginia Commonwealth University.

Virginia Commonwealth University, 2018

Major Director: Jeffrey L. Dupree, PhD, Anatomy and Neurobiology

Multiple sclerosis (MS), a demyelinating disorder of the central nervous system (CNS), affects approximately 400,000 individuals in the United States, and 2.5 million people worldwide. It is a leading cause of disability in young adults. Current treatments for MS target the inflammatory aspects of the disease, but do not aid in remyelination. To address remyelination as a therapeutic strategy, it is imperative to identify mechanisms that regulate

myelin formation, including epigenetic targets. In this study, we investigate the role of the *LMNA*, a gene encoding Lamins A and C, intermediate filaments of the nuclear lamina, in regulating oligodendrocyte development and myelination in the CNS. Using electron microscopic analyses, I examined levels of heterochromatin and its distribution in the oligodendrocyte nucleus as an indicator of gene expression, oligodendrocyte maturity, and myelin formation in the absence of A type lamins.. While overall levels of heterochromatin in oligodendrocytes were not altered in the absence of A type lamins, peripherally located heterochromatin was reduced and thinner myelin was observed in the spinal cord. My observations present novel findings for the role of *LMNA* in oligodendrocytes and myelination.

## INTRODUCTION

Multiple sclerosis (MS) is the primary demyelinating disease of the central nervous system (CNS), affecting approximately 2.5 million individuals worldwide, and 400,000 people in the United States with increasing prevalence (Ma et al., 2014). This chronic disease is the primary cause of nontraumatic neurologic disability in young adults, with the age of onset typically being between 20 and 40, and is three times more common in women than men (Auricchio et al., 2017; Smith et al., 2017). The National Multiple Sclerosis Society reports that estimated health care costs for a patient with MS range between \$18,000 to \$39,000 annually, with out of pocket costs for patients with insurance at \$2,000 annually. The annual cost in the United States is approximately \$28 billion (National Multiple Sclerosis Society; Ma et al., 2014).

Currently, there is no cure and all MS treatments fall into either the category of symptomatic treatments, known as nonspecific therapies, focusing on maintaining function and quality of life, or disease modifying treatments (DMTs), specific therapies, which aim to prevent relapse and delay progression of disability (Davies, 2007; Tullman 2013). There are no current therapies to restore demyelination that occurs in MS. To achieve this, a goal would be to target the oligodendrocyte to create new myelin. A plausible approach could involve finding a target that would upregulate myelin gene expression, by either targeting immature oligodendrocytes to develop into myelin generating cells, or by returning mature oligodendrocytes to their active myelinating state. To achieve the latter approach, it would be beneficial to identify factors that regulate myelin formation in order to target those factors in efforts to stimulate myelin repair. In

this study, we explore a candidate factor that potentially regulates gene expression in oligodendrocytes.

## **Multiple Sclerosis**

MS is an inflammatory autoimmune disease of the CNS. While the cause is yet unknown, it is believed to be a result of both environmental factors and genetic susceptibility. These factors trigger inflammation with resultant demyelination, oligodendrocyte death, axonal damage, gliosis, and neurodegeneration (Hartung et al., 2014). Initial symptoms of the disease can include: weakness in one or more limbs (35%), optic neuritis (20%), paraesthesiae (20%), diplopia (10%), vertigo (5%), disturbance of micturition (5%), and various other symptoms (5%) (Compston et al., 2008). Clinical subtypes of MS include relapsing-remitting MS (RRMS), secondary progressive MS (SPMS) and primary progressive MS (PPMS) (Abdelhack et al., 2017). Typically, MS follows a three stage progression. First is a pre-clinical stage where genetic and environmental factors have triggered the disease, only detectable through MRI; the second is marked by the RRMS subtype presenting with periods of demyelination and neurologic dysfunction, followed by remyelination and remission; and a third progressive stage, which either follows RRMS (SPMS), or progresses from onset (PPMS) (Baecher-Allan et al., 2018). The hallmark of MS pathology is the presence of focal demyelinated regions in the white matter; however, damage is also found in normal appearing white matter (NAWM) (Kutzelnigg and Lassman, 2014). In addition to demyelination, neuronal loss and atrophy are also seen in the gray matter, particularly that of the cortex (Peterson et al., 2001; Wegner et al., 2006). Remyelination following a demyelinating attack is an endogenous mechanism, occurring in acute and early

disease states,; however, repair becomes insufficient and eventually fails in late chronic disease, leading to progression of disability due to axonal degeneration (Frohman et al., 2006; Ozawa et al., 1994; Patrikios et al., 2006; Prineas et al., 1993;Stangel et al., 2017). Remyelination is conducted by adult oligodendroglial progenitor cells (OPCs) that differentiate into mature myelinating oligodendrocytes (Stangel et al., 2017). However, in chronic MS, differentiation of OPCs to myelinating oligodendrocytes is impaired (Kuhlmann et al., 2008).

### *Current Multiple Sclerosis Treatments*

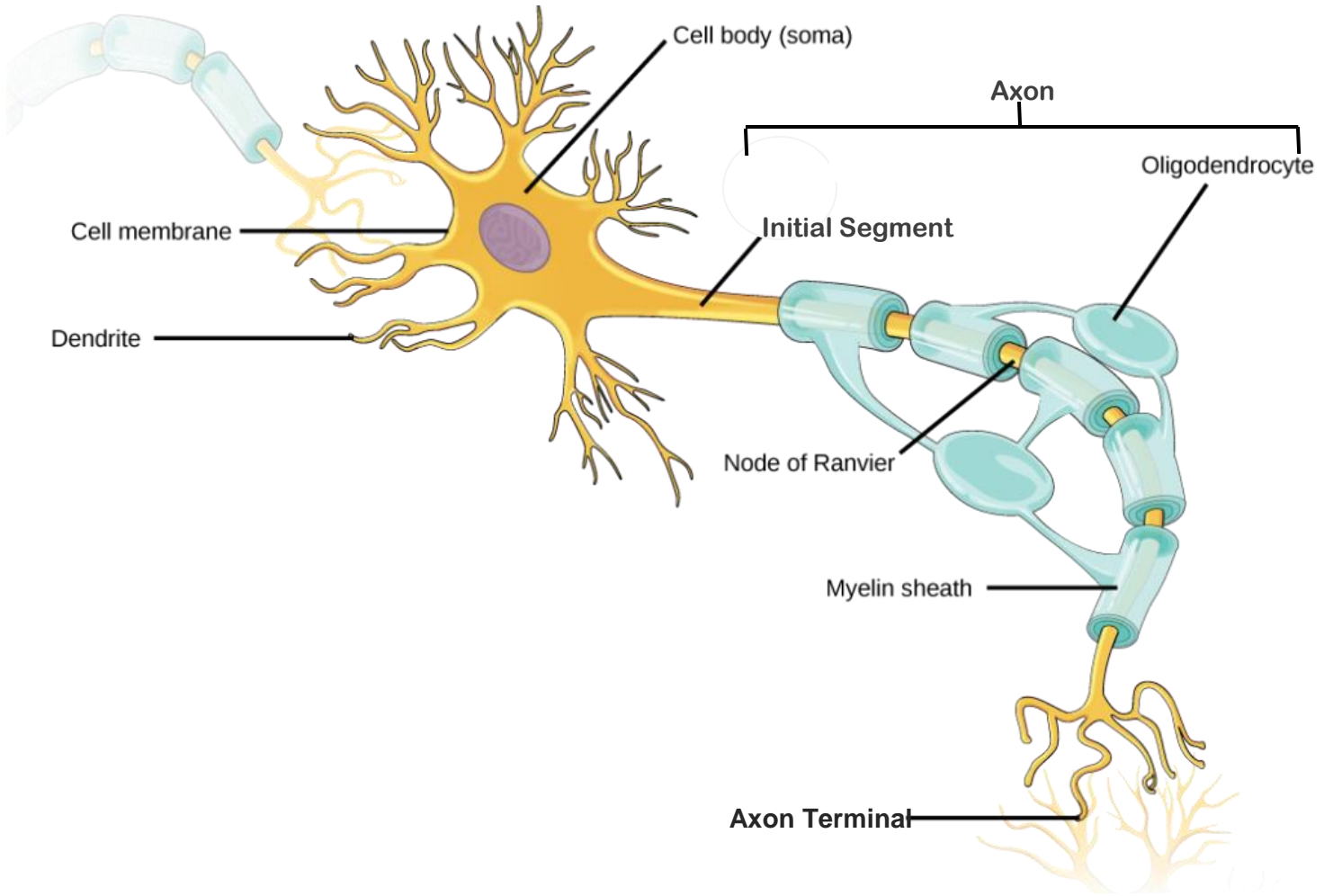
Disease modifying treatments are primarily concerned with controlling the inflammatory aspect of MS, but are less effective once the disease progresses to degeneration (Brück and Stadelmann 2003; Tremlett et al., 2004). At this time, there are 15 approved DMTs for MS, ranging in efficacy and safety (Smith et al., 2017). All currently available therapeutics target the immune system through either immunosuppression or immunomodulation (Dendrou et al., 2015; Hemmer et al., 2015). These current treatments increase quality of life, but come at the cost of suppressing the immune response. No available treatments facilitate myelin repair. Experiments with mouse models of MS have aided the identification and characterization of factors that influence remyelination, promoting OPC proliferation, migration, and differentiation (Gaesser and Fyffe-Maricich, 2016; Kremer et al., 2016; Stangel et al., 2017). By identifying candidate genes, transcription factors, and signaling molecules for remyelination, new therapeutic targets for MS can be explored.

## The Neuron

Neurons are cells of the nervous system specialized for intercellular communication and rapid electrical signaling. Typically, a neuron is comprised of a cell body, dendrites, and an axon, ending with the axon terminal (Figure 1.1). Dendrites are the target of chemical signaling, receiving synaptic input from the axon terminal of other neurons (Purves, 2012). Excitatory and inhibitory signals received from the dendrites are summed at the axon hillock, and depending on the result of this summation, an action potential is either fired or not from the axon initial segment (AIS) (Buttermore et al., 2013). The action potential is then propagated primarily through voltage-gated sodium channels (Hodgkin and Huxley, 1952; Hille, 2001; Quarles et al., 2006; Susuki and Rasband, 2008). An action potential is initiated when an influx of sodium ions through these channels is sufficient to reach threshold neuronal membrane potential, depolarizing the neuron and opening further voltage-gated sodium channels. As the action potential travels through the axon, the sodium channels close, and there is an efflux of potassium ions through the voltage-gated potassium channels, decreasing the membrane potential to hyperpolarization, and eventually returning to a resting potential, capable of propagating another action potential (Hodgkin and Huxley, 1952; Hille, 2001). Myelination of axons allows for more rapid and efficient action potential propagation in large caliber axons of the vertebrate nervous system (Tasaki, 1939; Foran and Peterson, 1992). In myelinated axons, action potentials are generated at the nodes of Ranvier (Verkhatsky and Butt, 2013) resulting in propagation of the electrical signal down the axon in a saltatory fashion. In addition to the nodes of Ranvier, the myelinated axon is divided into multiple domains including the paranode, where the myelin sheath is tethered to the axon, the juxtaparanode, where rectifying potassium channels cluster and the internode, which is the longest region of the myelinated axon (Verkhatsky and Butt, 2013).

**Figure 1.1. CNS Myelinated Neuron Schematic**

Synaptic input is received at the dendrites. Action potentials are initiated at the axon initial segment, and propagated along the axon through the internodes and generated at the nodes of ranvier in a saltatory fashion.



Adapted from Molnar and Gair (2012)

## **Oligodendrocytes**

Oligodendrocytes are the myelinating cells of the CNS. These cells extend multiple processes that ensheath axons in wraps of myelin, both along one axon and between multiple axons (Soldan and Pirko, 2012). One oligodendrocyte can extend from one to up to 30 myelinating processes, and oligodendrocyte subtypes, types I-IV, are categorized in relation to the number of processes they extend, as well as their morphology and size of the myelin sheaths they create (Bjartmar et al., 1994; Butt et al., 1995; Baumann and Pham-Dinh, 2001; Murtie et al., 2007). Because the largest caliber axons are myelinated first in postnatal development, types III/IV oligodendrocytes myelinate earlier, and types I/II myelinate the smaller caliber axons later (Butt et al., 1994; Hildebrand et al., 1993).

### *Oligodendrocyte Differentiation*

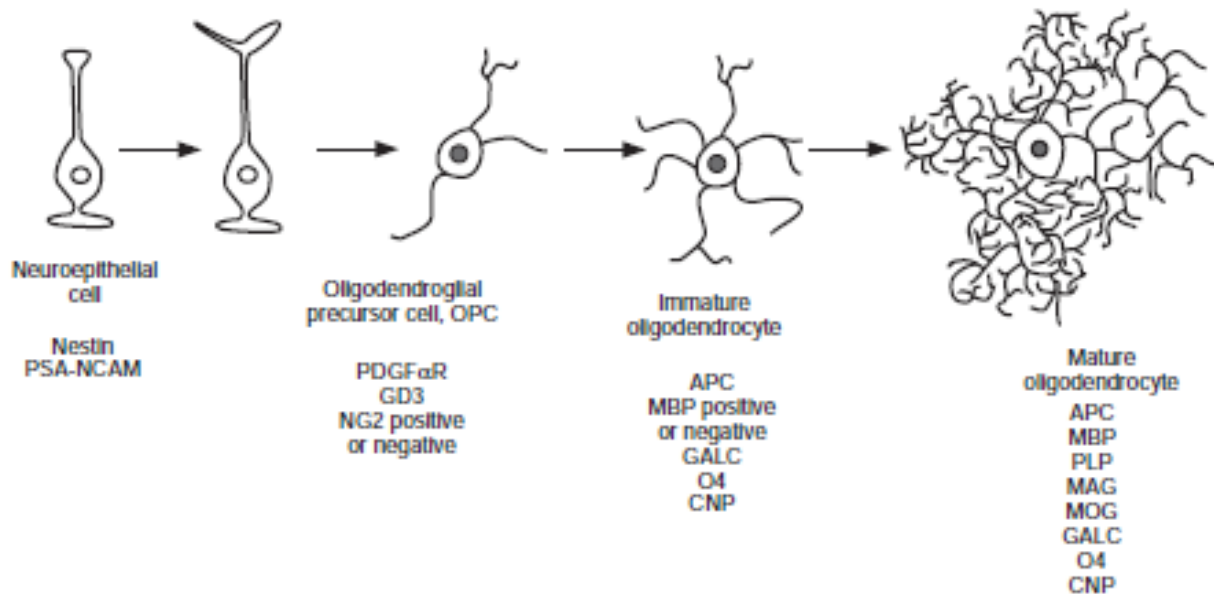
Oligodendrocyte progenitor cells (OPCs), resulting from multipotent neural stem cells (NSCs) in the subventricular zone (SVZ), generate oligodendrocytes (Richardson et al., 2006). These OPCs migrate from the SVZ to populate the CNS, and undergo proliferation and differentiation (Menn et al., 2006). Oligodendrocyte differentiation and maturation can be determined by antigenic markers (Figure 1.2). Additionally, some OPCs do not differentiate, and remain as adult OPCs or NG2-glia (Verkhatsky and Butt, 2013). These adult OPCs have the capacity to generate into oligodendrocytes, and can respond to demyelinating events (Menn et al., 2006). Oligodendrocyte maturity can also be identified based on characteristics seen in electron microscopy, dividing into three stages of maturity; 1. light, large cells with euchromatic nuclei and ample cytoplasm, 2. dark, smaller cells with more heterochromatic nuclei and 3. dense

, and medium cells, with characteristics between light and dark (Mori and Leblond, 1970). The euchromatic nuclei of oligodendrocyte progenitor cells have a relaxed chromatin structure, with greater DNA accessibility. This euchromatic state allows them to transduce signals to transcription factors, recruiting enzymes which activate or repress genes that regulate oligodendrocyte determination, proliferation, and migration (Liu et al., 2016).

In transitioning from the OPC to a premyelinating oligodendrocyte, genes involved in proliferation and the inhibition of differentiation are downregulated. As this process occurs, heterochromatin progressively forms, beginning at the nuclear periphery, among the nuclear lamina, and radiates towards the center of the nucleus (Liu et al., 2016). The localization of clumps of heterochromatin to the nuclear envelope is seen in mature myelinating oligodendrocytes, which also have the darker cytoplasm mentioned above, with a short endoplasmic reticulum and more prominent Golgi apparatus (Menn et al., 2006). It was reported that both in vitro and in vivo, histone deacetylase (HDAC) activity was required for oligodendrocyte differentiation, with a model of differentiation characterized by progressively decreasing inhibitors of transcription, upregulating activators, followed by myelin gene expression (Liu and Casaccia, 2010).

### **Figure 1.2. Oligodendrocyte Development**

As a neuroepithelial cell develops into a mature myelinating oligodendrocytes, different genes are expressed. Stages of development of an oligodendrocyte can be identified by the oligodendrocyte and myelin genes the cell expresses.



Adapted from Verkhatsky and Butt (2013)

## **Myelin**

Myelination increases conduction velocity in axons by acting as an electrical insulator, through a reduction in capacitance and an increase in resistance (Verkhatsky and Butt, 2013). In the CNS, oligodendrocytes extend multiple processes to myelinate several axons, whereas in the peripheral nervous system (PNS), Schwann cells extend a single myelinating process. Myelin is composed of multiple layers of membranes wrapped around the axon (Purves, 2012). Unique to myelin is the composition of these layers. In contrast to most other biological membranes, composed of approximately 45% lipid and 55% protein, myelin is composed of approximately 70% lipid and 30% protein (Baumann and Pham-Dinh, 2001; Quarles et al., 2006). Additionally, myelin has low water content, allowing it to be an efficient insulating material (Baumann and Pham-Dinh, 2001). Due to the insulating capacity of myelin, myelinated axons have conduction velocities of up to 150 meters per second, as opposed to the conduction velocities of unmyelinated axons, ranging from 0.5 to 10 meters per second. The myelin sheath is not a continuous structure but is composed of segments that align along the axon. These segments can be as long as 1mm and adjacent segments are separated by short (1-2  $\mu\text{m}$ ) myelin bare regions known as node of Ranvier. Action potential propagation is restricted to the nodes of Ranvier resulting in the electrical signal passing from node to node resulting in action potential propagation called saltatory conduction (Purves, 2012).

### *CNS Myelin*

As stated above, myelin is composed of 70% lipid and 30% protein. In the CNS, the predominant myelin proteins are proteolipid protein (PLP), isoform DM-20, and myelin basic

protein (MBP), which together constitute about 80% of the proteins in the CNS myelin sheath (Campagnoni and Macklin, 1988). The remaining 20% of proteins of the CNS myelin sheath include higher molecular weight proteins including myelin associate glycoprotein (MAG) and 2':3'-cyclic nucleotide 3'-phosphodiesterase (CNP) (Eng et al., 1968).

### *Myelination in the Murine CNS*

Myelination begins at birth in the mouse spinal cord, and is completed in all areas between postnatal day (PND) 40-60 (Baumann and Pham-Dihn, 2001; Snaidero and Simons, 2014). Beginning in the spinal cord, myelination proceeds in a rostral to caudal gradient and is mostly complete in the mouse CNS by PND 60 (Foran and Peterson, 1992). Myelination reaches its peak in the spinal cord at PND 20 (Benjamins and Morell, 1978), while peak levels of myelination continue until PND 45 in the mouse corpus callosum (Sturrock, 1980). Larger caliber axons are myelinated first, with smaller diameter axons not beginning myelination until PND 20 (Hildebrand et al., 1993). In the mouse optic nerve, there are two bursts of peak myelination. The first wave begins at the 3<sup>rd</sup> week of life, and the second wave initiates at postnatal week 5, accounting for a threefold increase in the number of myelinated nerve fibers present at week 3 (Dangata et al., 1996).

## Chromatin and Gene Expression

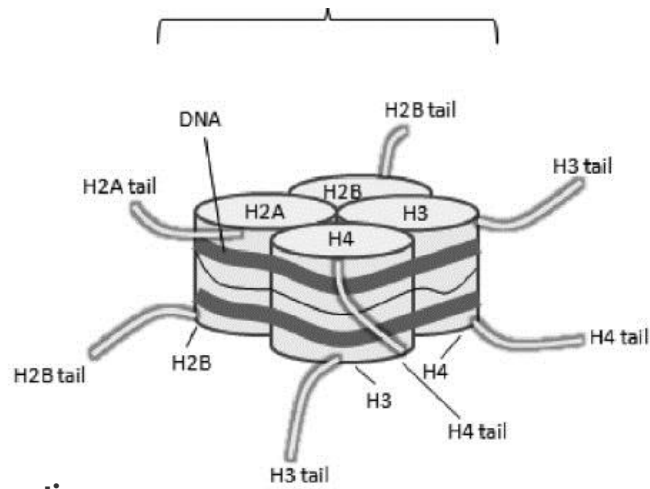
One mechanism by which myelin genes are expressed is through epigenetic regulation of chromatin. Chromatin packages genetic material in a complex of proteins and DNA in the nucleus of the cell. Its structure is dynamic, and these changes affect gene expression (Felsenfeld and Groudine, 2003). It is a complex of DNA and proteins, with repeating units called nucleosomes, composed of DNA wrapped around an octamer of histone proteins (McGinty and Tan, 2014). How tightly these nucleosomes are packaged affects the ability of DNA binding factors to bind to DNA and impacts transcription (McGinty and Tan, 2014) (Figure 1.3). Based on the packaging of the DNA and the associated proteins, chromatin is referred to as heterochromatin and euchromatin. Heterochromatin is tightly packaged, making it inaccessible to DNA binding factors, and generally transcriptionally silent (Cockell and Gasser, 1999; Nielsen et al., 2002; Copray et al., 2009). In addition to the tight packaging of heterochromatin playing a role in transcription regulation, the position of the heterochromatin within the nucleus appears to regulate gene expression as a peripheral location, and consequently an association with nuclear envelope lamins, results in an environment of repressive gene expression (Politz et al., 2013). In an electron micrograph, heterochromatin appears dark consistent with increased density of the DNA and associated proteins. Such dense packaging is consistent with heterochromatin being less transcriptionally active. In contrast, euchromatin has a more relaxed and less tightly packaged structure and is associated with transcriptionally active DNA. (Fernandez et al., 2012). Also consistent with this more relaxed packaging, euchromatin, in an electron micrograph, appears light or electron lucent.

Histone modifications impact whether chromatin is heterochromatic or euchromatic, with acetylation of histone 3 lysine 9 (H3K9) and methylation of histone 3 lysine 4 (H3K4) being characteristic of euchromatin, and H3/H4 deacetylation, and methylated H3K9 characteristic of heterochromatin (Wallrath et al., 2014). HDACs remove acetyl groups from histones, and are associated with transcriptional repression (Braunstein et al. 1993; Braunstein et al. 1996; Gregoret et al. 2004; Hernandez and Casaccia, 2016).

**Figure 1.3. Chromatin Structure**

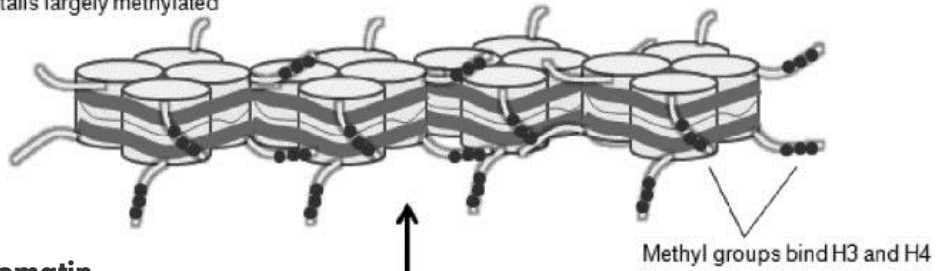
Chromatin is composed of repeating units called nucleosomes. Heterochromatin is composed of condensed nucleosomes, creating a primarily repressive environment. Euchromatin is a more relaxed chromatin structure, where DNA is accessible to DNA binding factors.

## Nucleosome



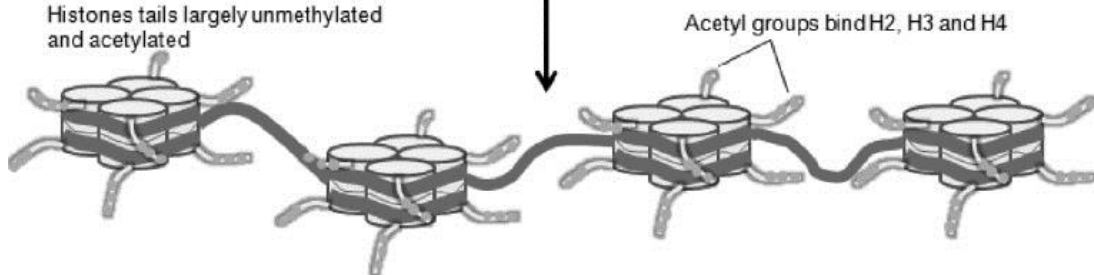
### Heterochromatin

**Condensed nucleosomes:**  
Histones tails largely methylated



### Euchromatin

**Uncondensed nucleosomes:**  
Histones tails largely unmethylated and acetylated



Adapted from Saini et al. (2013)

## **Nuclear Lamina**

Located beneath the inner nuclear membrane is the nuclear lamina, an intermediate filament meshwork, comprised mainly of type V intermediate filament proteins known as lamins, including lamins A, C, B1, and B2 (Young et al., 2012; Steensel and Belmont, 2017). Adjacent to the nuclear lamina is a layer of heterochromatin, which creates a primarily repressive environment (Fawcett, 1966). Both A and B type lamins tether this heterochromatin to the nuclear periphery, (Politz et al., 2013). Interacting with the nuclear lamina, are lamina-associated domains (LADs). LADs are genomic regions, relatively poor in actual genes, with those gene within the LAD being expressed at very low levels. They are involved in guiding the folding of chromosomes in the nucleus (Yanez-Cuna and Steensel, 2017). There are two different types of LADs, constitutive and facultative. Constitutive LADs are highly conserved across species and present in all cell types. They are rich in A/T sequences, thought to anchor to the nuclear lamina, and provide structural backbone for interphase chromosomes (Meuleman et al., 2013). Facultative LADs are associated with the nuclear lamina only in some cell types. During differentiation, genes located in facultative LADs either move away from the nuclear lamina, correlating with activation, or towards it, correlating with inactivation (Yanez-Cuna and Steensel, 2017).

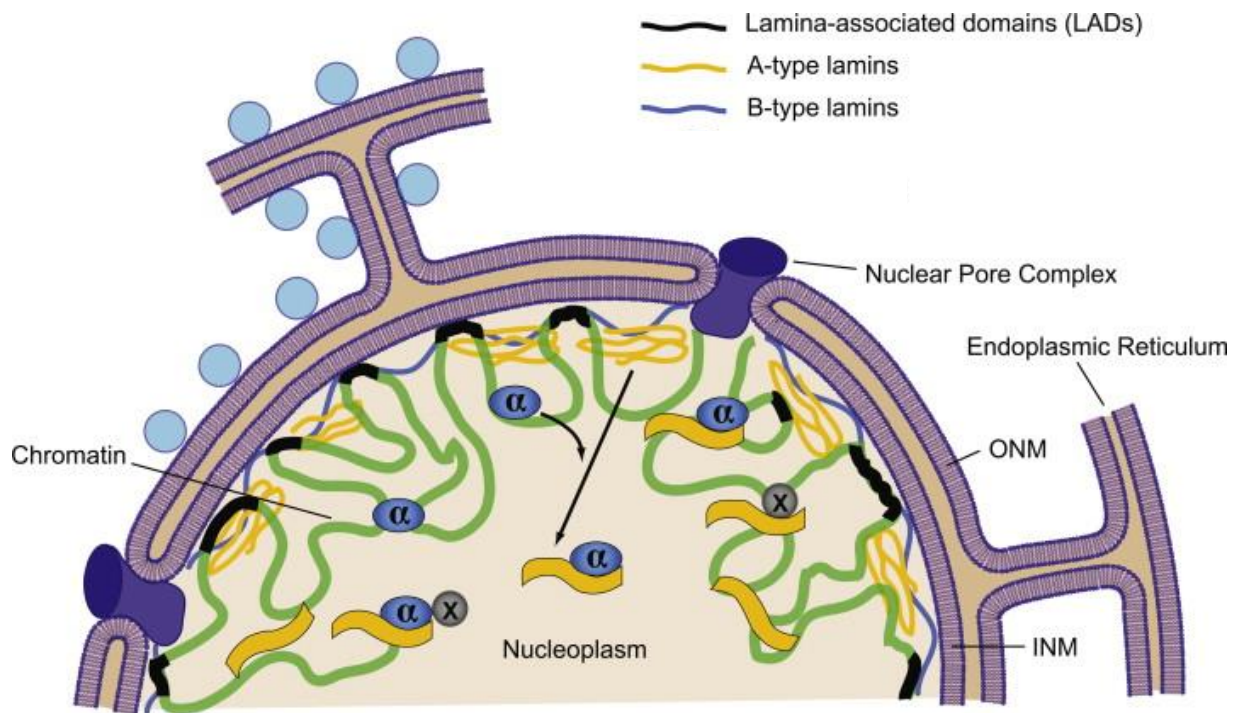
## **Lamins**

Nuclear lamins are intermediate filaments that are components of the nuclear lamina (Young et. al., 2012). The lamins act as a scaffold for protein complexes involved in nuclear structure and function, and impact signaling pathways, transcription factors, and chromatin

associated proteins (Andres and Gonzales, 2009) (Figure 1.4). There are two types of lamins: A type and B type. There are two B type lamins and they are encoded by separate genes, with *LMNB1* encoding lamin B1, and *LMNB2* encoding lamin B2 (Biamonti et al., 1992; Lin and Worman, 1995). A type lamins are encoded by the gene *LMNA*, which produces prelamin A, the precursor to mature lamin A, and lamin C, by alternative splicing (Lin and Worman, 1993). Both A and B type lamins are able to bind chromatin via carboxyl-terminal tail domains (Taniura et al., 1995).

**Figure 1.4. Lamins and the Nuclear Envelope**

A type and B type lamins act as a scaffold for protein complexes involved in nuclear structure and function, and interact with chromatin both directly and through lamina associated domains .



Adapted from Gesson et al. (2014)

### *B Type Lamins*

The intron-exon structure for lamins B1 and B2 is similar presenting with a conserved amino acid sequence of approximately 60% suggesting that they are a result of gene-duplication (Biamonti et al., 1992; Davies et al., 2011; Jung et al., 2013; Lin and Worman, 1995). In vitro studies have elucidated roles of B type lamins in DNA replication, mitotic spindle formation, and gene transcription (Belmont et al., 1993; Moir et al., 1994; Tsai et al., 2006). B type lamins are thought to primarily associate with heterochromatic, gene poor regions (Adam and Goldman, 2012). Lamin B2 has been found to be essential for neuronal migration in the developing brain. A duplication of *LMNB1* has been linked to Autosomal Dominant Leukodystrophy (ADLD), a fatal demyelinating disease (Padiath et al. 2006). Overexpression of *LMNB1* in oligodendrocytes has been found to cause epigenetic changes, resulting in down regulation of lipogenic gene expression and loss of myelin-enriched lipids (Padiath et al., 2016). This displays a role of lamin function in oligodendrocytes in disease.

### *A Type Lamins*

A type lamins are encoded by the gene *LMNA*, which produces prelamin A, the precursor to mature lamin A, and lamin C, by alternative splicing (Lin and Worman, 1993). The amino acid sequences of prelamin A and lamin C are identical for the first 566 residues, but prelamin A terminates with exon 12 sequences with 98 unique residues and a CAAX motif, which functions to target lamin A to the nuclear periphery (Holtz et al., 1989), whereas lamin C terminates with exon 12 sequences and 6 unique amino acids (Young et al., 2012). The post translational modification from prelamin A to mature lamin A clips the terminal 14 amino acids (Young et al.,

2012). A type lamins are expressed only at low levels during development, and lamin A and C proteins are not detectable in the brain until PND 15, with expression increasing with maturation (Roeber et al., 1989). A type lamins interact directly with chromatin at the nuclear periphery (Dorner et al., 2007). While both B and A type lamins tether heterochromatin to the nuclear periphery, A type lamins are developmentally regulated, implicating a dynamic role of peripheral heterochromatin in development associated with them (Politz et al., 2013). Additionally, A type lamins associate with several transcriptional repressors (Hutchison and Worman, 2004; Gotzmann and Foisner, 2005; Maraldi et al., 2006). In the absence of *LMNA*, peripheral heterochromatin is reduced, and an inversion of the localization from the periphery to the nuclear interior is seen (Galiová et al., 2008). Several genetic diseases caused by mutations in *LMNA*, called laminopathies, have been identified, and linked to over 180 mutations in *LMNA* (Zhang et al., 2013). Laminopathies include cardiomyopathy, peripheral neuropathy, madibulocral dysplasia, partial lipodystrophy, and several forms of muscular dystrophy (Jung et al., 2013). Barateau et al. (2017) discovered a point mutation in the *LMNA* gene that resulted in the inability of A type lamins to target to the nuclear envelope. Their findings showed that in the absence of A type lamins at the nuclear envelope due to this point mutation, acetylation of H3K9 was increased, which is associated with transcriptionally active euchromatin (Wallrath et al., 2014).

### *LMNA Null Mutant*

The *LMNA* null mutant mouse results in ablation of both lamins A and C (Zhang et al., 2013). These mice display cardiac arrhythmia, reduced fat stores, growth retardation, and abnormal emerin targeting (Sullivan et al., 1999). However, at birth, the *LMNA* knockout (KO)

is indistinguishable from wild type (WT) littermates (Sullivan et al., 1999). *LMNA* KO mice display hindered growth by 2-3 weeks of age, clinical features of muscular dystrophy by 4-6 weeks of age, and do not survive past 8 weeks of age (Nikkolova et al., 2004). Mutant mice deficient in only lamin A, prelamin A, or lamin C have been created, and do not have lethal phenotypes, suggesting that A type lamins can play compensatory roles for one another (Zhang et al., 2013).

### **Project Aim**

The goal of this study is to elucidate the role of A type lamins in oligodendrocytes. Previous studies have shown that A type lamins play an essential function in chromatin architecture, tethering chromatin to the nuclear periphery, and impacting gene expression. Because remyelination in MS requires the differentiation of adult OPCs to mature myelinating oligodendrocytes, it is essential to identify candidate genes that impact this differentiation. Because A type lamins are associated with tethering chromatin and regulators of gene expression, it was of interest to study the impact on oligodendrocyte heterochromatin and CNS myelin. It was hypothesized that heterochromatin levels would be reduced in oligodendrocytes, specifically at the nuclear periphery. Because previous studies have shown increased acetylation of H3K9, associated with active euchromatic chromatin, in the absence of A type lamin targeting to the nuclear periphery, and because A type lamins bind transcriptional repressors, I postulated that ablation of *LMNA* would increase myelin gene expression in oligodendrocytes, resulting in increased myelination in the CNS. Using a total *LMNA* null mutant mouse, ratios of total

heterochromatin to nuclear area, as well as peripheral heterochromatin to nuclear area, and ratios of peripheral heterochromatin as related to total heterochromatin were measured to understand how the absence of A type lamins affects heterochromatin distribution in the oligodendrocyte nucleus in the corpus callosum, spinal cord, and optic nerve. The resultant impact of ablation of *LMNA* on myelination in the corpus callosum and spinal cord was studied using g-ratios as a measure of myelin thickness with regard to axon caliber. Additionally, oligodendrocyte nuclear area to total cell body area was measured to determine if A type lamins play a role in oligodendrocyte maturity.

## MATERIALS AND METHODS

### **Animals**

Lamin A (*LMNA*) knockout (KO) and wild type (WT) mice were bred and maintained in the Mount Sinai School of Medicine Animal Facility vivarium, which is an AAALAC accredited facility. The mice were generated by heterozygous X heterozygous matings resulting in litters containing WT, KO and heterozygous littermates. Food and water for the mice were provided *ad liberatum*. All mice were maintained on a 12 hour light/12 hour dark alternating cycle. For this study, only the KO and WT mice were analyzed while the heterozygous mice were used to maintain the colony. Homozygous KO mice have a shortened lifespan and rarely survive past 50 days of age. For this reason, all analyses were restricted to either PND 21 or PND 35. All analyses were conducted in a blinded manner and the genotypes of the mice were not revealed until all quantitative analyses were completed.

### **Perfusion**

Mice were perfused in the laboratory of Dr. Patrizia Casaccia at Mount Sinai School of Medicine according to the protocol established in our laboratory (Marcus et al., 2006; Shroff et al., 2009). Briefly, mice were deeply anesthetized using a combination of corneal reflex and toe pinch to confirm. Mice were placed on a perfusion rack in a prone position. A “Y” shaped incision cutting through the ribs and diaphragm was used to expose the heart. A 22 gauge needle was inserted into the left ventricle and 0.9% saline was used to flush the blood. A small incision

was made in the right atrium to allow the perfusate to exit the body. The saline solution was flushed through the animal until the saline perfusate ran clear and the liver blanched. Following the saline perfusate, the mice were perfused with a solution of 0.1 M sodium cacodylate buffer (pH 7.3) containing 4% paraformaldehyde (Polyscience, Warrington, PA) and 5% glutaraldehyde (Electron Microscopy Sciences, Hatfield, PA) at a rate of 7-10 ml/minute. The aldehyde fixative was run through the animal for 25 minutes after muscle contractions ceased. Animals were stored for 2 weeks at 4°C in the same aldehyde fixative. Since the mice were perfused in the Casaccia laboratory, the mice were shipped to our laboratory during this two week post fixation period. Mice were placed in 50ml conical centrifuge tubes; the tubes were tightly capped and the caps were wrapped in parafilm (Bemis North America, Neenah, WI). Upon arrival, the mice were immediately transferred to the refrigerator for the remaining period of the two weeks post fixation period.

### **Electron Microscopy Tissue Processing**

Following two weeks of post fixation in the aldehyde fixative, spinal cord, optic nerve and corpus callosum samples were prepared for transmission electron microscopic analysis. Briefly, the entire brain and spinal cord and the optic nerve, from the level of the optic canal anteriorly to ~2mm posterior to the optic chiasma, were harvested from each mouse. These samples were incubated in 0.1M sodium cacodylate in a 20ml scintillation vial overnight at 4°C. The next day spinal cord samples at the level of cervical region C2-4, the whole brain and optic nerve 0.5 cm anterior to the optic chiasm were placed in a fresh rinse of 0.1M sodium cacodylate buffer. The cacodylate rinses removed excess aldehydes to prevent their reaction with osmium

tetroxide in subsequent tissue processing steps. For the corpus callosi, a sagittal brain matrix was used to make a mid sagittal cut separating the two hemispheres, and then two additional sagittal cuts positioned 1mm lateral to the mid sagittal cut were made to generate 1mm sagittal sections. These two sagittal sections immediately lateral to midline were used for corpus callosi analysis. The day after the tissue was grossly dissected, samples were additionally post fixed in 1% osmium tetroxide (Electron Microscopy Sciences, Hatfield, PA) in 0.1M cacodylate buffer (pH 7.3), and gently rotated for one hour to ensure optimal fixative penetration. Following the osmium tetroxide post fixation, samples were rinsed three times for five minutes per rinse in 0.1M cacodylate. All processing steps involving osmium tetroxide were conducted under a chemical fume hood. Osmium tetroxide waste was reacted with vegetable oil to reduce fix waste for disposal. Tissue samples were dehydrated using increasing concentrations of ethanol ranging from 30% to 100%. For the final two 100% ethanol rinses, “dry” ethanol, ethanol stored on molecular sieve was used. Two 30-minute rinses of the transition solvent, propylene oxide (Electron Microscopy Sciences, Hatfield, PA), were conducted prior to the overnight incubation in a solution of one part propylene oxide and one part PolyBed resin (PolySciences, Warrington, PA). The following day, the tissue was incubated in 100% PolyBed resin for 24 hours with constant agitation at room temperature.

After the 24-hour incubation in PolyBed resin, optic nerve and spinal cord samples were placed in flat embedding molds while the corpus callosal samples were placed in inverted Beem capsules (Electron Microscopy Sciences, Hatfield, PA). All tissue samples were embedded in freshly prepared 100% PolyBed resin and polymerized at 60° C for 36 hours.

One micron and 90 nm sections were cut for each sample. One micron sections were stained with toluidine blue and qualitatively assessed to confirm correct region of interest, orientation, and fixation quality using a Zeiss AxioImager A1 (Zeiss Microscopy, Inc; Englewood NY). The 90 nm sections were placed on 200 mesh copper grids and stained with uranyl acetate and lead citrate.

### **Image Collection Using Transmission Electron Microscopy**

Sections were imaged using either a JEOL JEM 1230 transmission electron microscope (TEM), equipped with a Gatan Orius SC 1000 camera or a JEOL JEM 1400Plus TEM equipped with a Gatan Ultra Scan CCD camera. Spot size was 2, and the high tension setting was 100Kv with the filament set below saturation. The desired area of the corpus callosum was identified as the region of myelinated axons with myelinated axons in cross section that were located between the myelinated axons in longitudinal orientation, positioned inferior to cortical layer 6, and superior to the lateral ventricle. For the spinal cord, all images of myelinated axons were collected from the ventral column, which was identified by large myelinated axons and the presence of the posterior median sulcus. The motor horn motor neurons were identified as the large neurons in the grey matter regions located lateral to the ventral columns.

Oligodendrocytes were identified on electron micrographs by their dense cytoplasm and nucleus, and absence of intermediate filaments and glycogen. For morphologic analysis, 10 oligodendrocytes per region were imaged using transmission electron microscopy. Images in the corpus callosum were collected from four littermate pairs of PND 21 animals, and three LMNA knockout and four wild type littermates of PND 35 mice. Oligodendrocyte images in the spinal

cord were collected from 5 littermate pairs of PND 21 and four littermate pairs of PND 35 animals. Images of oligodendrocytes in the optic nerve were collected from 3 littermate pairs of PND 35 animals.

To identify oligodendrocyte specific effects, imaged spinal cord neurons were collected from PND 21 animals (n=5); images of cortical neurons (n=3) and spinal cord neurons (n=4), as well as astrocytes from the optic nerve (n=4) were collected from PND 35 animals. Neurons were identified as large cells in grey matter regions, in combination with the presence of intermediate filaments without tight bundling, and the presence of a large nucleus with a prominent nucleolus. Astrocytes were identified based on the presence of glial fibrillary acidic protein (GFAP) and glycogen.

### **Heterochromatin analysis**

Electron microscopy images of oligodendrocytes from the corpus callosum (n=4) and spinal cord (n=5), as well as spinal cord neurons (n=5) of PND 21 animals were collected and analyzed. For PND 35 animals, oligodendrocytes were analyzed from the optic nerve (n=4), corpus callosum (n=4), and spinal cord (n=5), as well as cortical (n=3) and spinal cord (n=4) neurons, and optic nerve astrocytes (n=4). Images were analyzed using Image J (NIH), according to the protocol that I established and published in Liu et al. (2012). Briefly, using the freehand tracing tool, outlines were manually traced around the nuclei, and area (in pixels) was measured (Figure 2.1). The area outside of the nucleus was cut from the image (Figure 2.2). The nucleolus was traced, measured, and cut from the image, and the area of the nucleolus was subtracted from total nuclear area (Figure 2.3). Using the thresholding tools, heterochromatic

areas were identified by their observably darker appearance above background, and selected on a gradient of 0 to 256 grey scale. Due to the variation among sections, a consistent range of thresholding could not be set across all images. However, there was less variation in saturation between images of the same section and thresholding was set within a range of approximately 20 values on a grey scale, a variation of 8% (Figure 2.4). Peripheral heterochromatin, defined as heterochromatic regions contiguous with the nuclear envelope, was traced with the freehand tool (Figure 2.5). The area inside this selection was cropped from the image. Peripheral heterochromatin was selected and measured using the thresholding tool, set to the same grayscale value as the thresholding of total heterochromatin (Figure 2.6). Ratios of total heterochromatin to total nuclear area, peripheral heterochromatin to total nuclear area, and peripheral heterochromatin to total heterochromatin were calculated.

Ratios were statistically compared between wild type and *LMNA* knockout mice using an unpaired, two-tailed student's t-test ( $p < 0.05$ ) to determine if the means of the ratios for each analysis were significantly different between WT and *LMNA* KO. Statistical analyses were carried out using Prism 7 (GraphPad Software, Inc.).

**Figure 2.1. Selection of oligodendrocyte nuclear area**

The oligodendrocyte nucleus was traced using the freehand tool, and its area was measured in pixels.

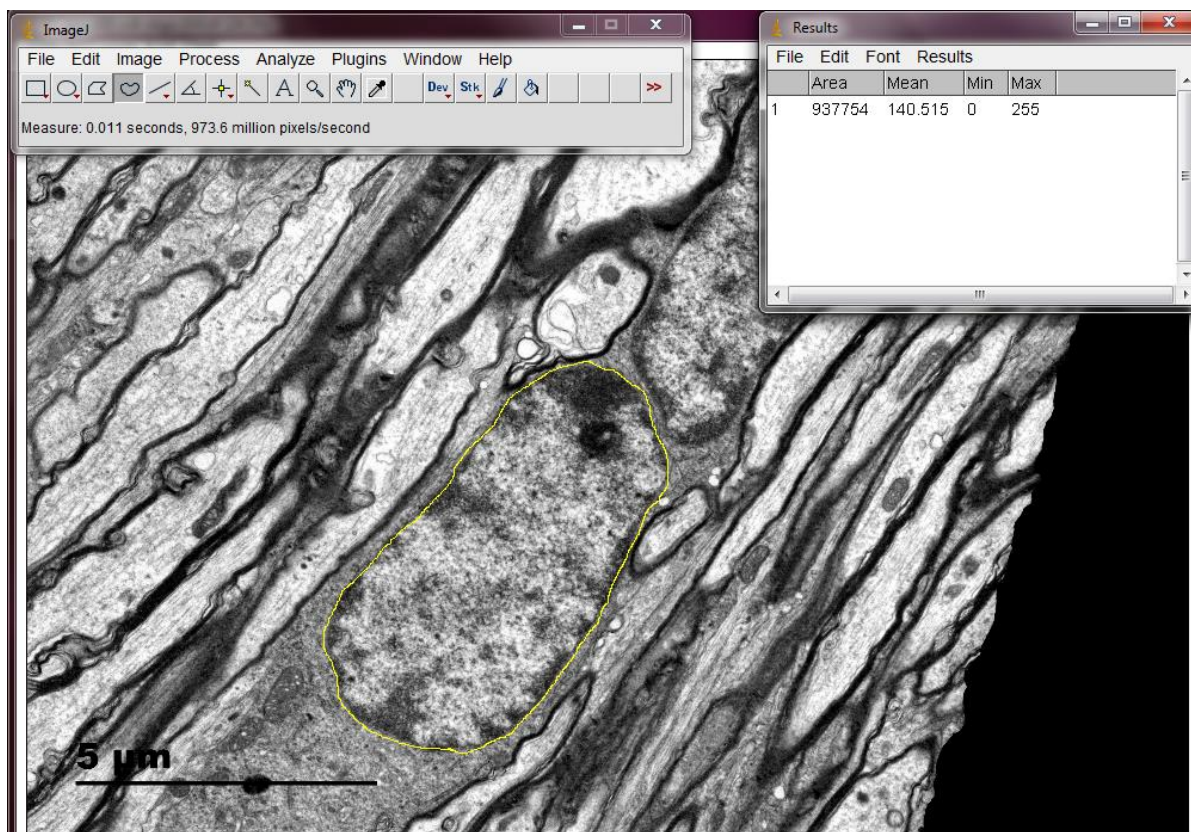


**Figure 2.2. Isolation of oligodendrocyte nuclear area**

The area outside the nucleus was cleared from the image.

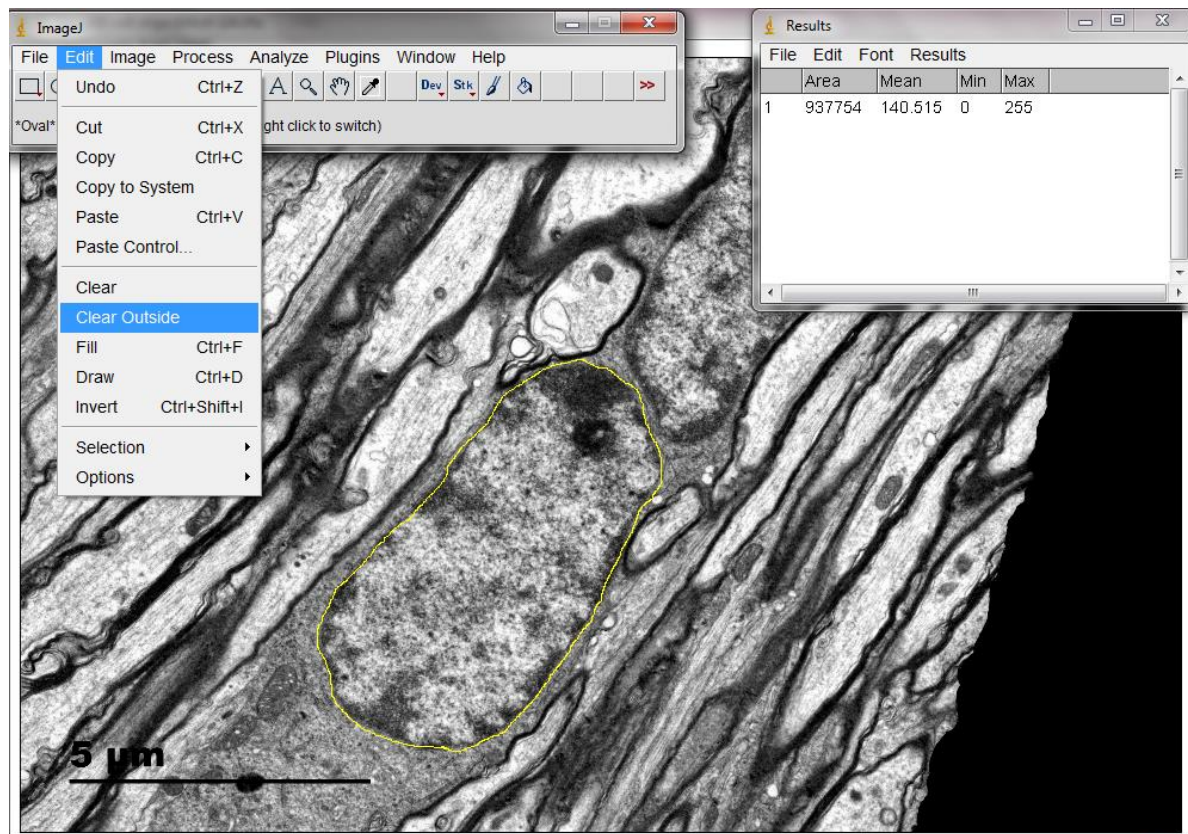


**Figure 2.3. Selection and elimination of nucleolus from analysis**

The nucleolus was traced using the freehand tool and measured in pixels. That measurement was subtracted from the total nuclear area for analysis. The nucleolus was then cleared from the image.

The screenshot displays the ImageJ software interface. The main window shows a grayscale image of a biological specimen, likely a cell or tissue section, with a yellow selection box highlighting a small region. The status bar at the bottom of the main window indicates the coordinates and value of the selected pixel:  $x=1760, y=931, \text{value}=255$ .

The Results window is open, displaying a table of data for the selected region. The table has the following structure:

	Area	Mean	Min	Max
1	937754	140.515	0	255
2	12369	36.204	0	215

**Figure 2.4. Thresholding and selection of heterochromatin**

Using the thresholding tool, with a gray scale of 0 to 256, heterochromatic regions identified as regions dramatically darker than background levels were selected and measured in pixels.

The screenshot displays the ImageJ software interface. The main window shows a red and white thresholded image of a cell. The 'Results' window is open, displaying a table of analysis data. The 'Threshold' dialog box is also visible, showing a histogram and various settings.

**ImageJ**  
File Edit Image Process Analyze Plugins Window Help  
Measure: 0.033 seconds, 324.5 million pixels/second

**Results**  
File Edit Font Results

	Area	Mean	Min	Max
1	937754	140.515	0	255
2	12369	36.204	0	215
3	313888	80.734	0	118

**Threshold**  
0  
118  
Default Red  
 Dark background  Stack histogram  
Auto Apply Reset Set

**Figure 2.5. Peripheral heterochromatin selection**

Peripheral heterochromatin was traced using the freehand tool.

The screenshot displays the ImageJ software interface. The main window shows a grayscale image of a biological specimen, which has been thresholded to produce a red and white binary image. The red areas represent the foreground, and the white areas represent the background. The thresholding process is visualized in the 'Threshold' dialog box, which shows a histogram of the image with a vertical line indicating the threshold value. The 'Results' window displays the following data:

Area	Mean	Min	Max
937754	140.515	0	255
12369	36.204	0	215
313888	80.734	0	118

The 'Threshold' dialog box includes a histogram, a threshold slider, and options for 'Dark background' and 'Stack histogram'. The 'Results' window has a menu bar with 'File', 'Edit', 'Font', and 'Results'.

**Figure 2.6. Peripheral heterochromatin isolation and thresholding**

The area inside the peripheral heterochromatin was removed from analysis, and peripheral heterochromatin was selected with the thresholding tool at the level established in Figure 2.4, and measured in pixels.

The screenshot displays the ImageJ software interface. The main window shows a grayscale image of a cell with a red threshold mask overlaid on its boundary. The 'Results' window is open, displaying a table of analysis data for four regions of interest. The 'Threshold' dialog box is also visible, showing a histogram of the image with a red threshold line set at 118. The 'Threshold' dialog has 'Default' selected for the mode and 'Red' for the color. The 'Dark background' and 'Stack histogram' options are unchecked. The 'Auto', 'Apply', 'Reset', and 'Set' buttons are visible at the bottom of the dialog.

	Area	Mean	Min	Max
1	937754	140.515	0	255
2	12369	36.204	0	215
3	313888	80.734	0	118
4	168775	71.208	0	118

## **G-Ratio Analysis**

Electron microscopy images were collected of myelinated axons from the spinal cord (n=5) and corpus callosum (n=3) of PND 21 animals, and from the spinal cord (n=3) and corpus callosum (n=4) of PND 35 animals. All myelinated axons in an image were measured, until a minimum of 100 myelinated axons were measured per animal. Axon caliber was calculated by averaging the measurement of the longest diameter of an axon and the shortest, in pixels. Axon caliber was converted from pixels to microns by dividing the number of pixels in the axon caliber measurement by the number of pixels per micron as determined by measuring the scale bar of the image. Myelin thickness was calculated by measuring the thickest and thinnest region of the myelin sheath using only areas of the sheath that were compacted, showed no signs of fixation artefact and were not cut at an angle. Total fiber caliber was calculated by adding the two myelin thicknesses to the axon caliber value. G-ratios were calculated by dividing the axon caliber (in pixels) by the total fiber caliber (in pixels). G-ratios were plotted in a scatter plot with g-ratios on the y-axis, and axon caliber (in microns) on the x-axis. Linear regression analyses were performed in Prism 7 to determine if the slopes of the WT and *LMNA* KO differed, and an unpaired Student's t-test was performed to compare the g-ratio means ( $p < 0.05$ ).

## **Measurement of nucleus : cytoplasm ratio**

Electron microscopy images of oligodendrocytes from the corpus callosum (n=4) and spinal cord (n=5) of PND 21 animals, and from the optic nerve (n=3), corpus callosum (n=4), and spinal cord (n=4) of PND 35 animals were analyzed. Using Image J (NIH) software, outlines were traced around the cell body of oligodendrocytes (excluding processes), and the

total cell area (in pixels) was measured. The area of the nucleus, obtained from heterochromatin analysis, was subtracted from the total cell area to calculate the area of the cytoplasm. The ratio of nuclear area to area of the cytoplasm was calculated and compared using an unpaired Student's t-test ( $p < 0.05$ ).

## RESULTS

### **No difference was observed in heterochromatin ratios or distribution in the oligodendrocyte nucleus of PND 21 WT and *LMNA* KO mice**

I hypothesized that ablation of the Lamin A (*LMNA*) gene would result in improper targeting of heterochromatin to the nuclear periphery. To test this hypothesis, we analyzed oligodendrocytes from the spinal cord and corpus callosum of wild type and *LMNA* knockout mice at PND 21.

#### *Heterochromatin Distribution in the Corpus Callosum of PND 21 Mice*

No significant difference in ratios of total heterochromatin to total nuclear area was observed in oligodendrocytes in the corpus callosum of PND 21 mice (Figure 3.1). Ten oligodendrocytes, identified based on ultrastructural features unique to these CNS myelin forming cells, were analyzed per mouse. The mean heterochromatin to nuclear area of WT oligodendrocytes was  $0.361 \pm 0.009$  (n=4), and the mean of the KO heterochromatin ratios was  $0.369 \pm 0.016$  (n=4) (t test p = 0.40). Additionally, no difference was observed between the means of the ratios of peripheral heterochromatin in the nucleus of WT mouse corpus callosum oligodendrocytes  $0.194 \pm 0.011$  and KO  $0.200 \pm 0.027$  ( t test p = 0.72). The means of the ratios of peripheral heterochromatin to total heterochromatin were also not significantly different between oligodendrocytes in the corpus callosum of PND 21 mice. The corpus callosum

oligodendrocytes of WT mice had a mean peripheral heterochromatin to total heterochromatin ratio of  $0.539 \pm 0.023$ , and KO mice had a mean of  $53.1\% \pm 6.6\%$  (t test  $p = 0.83$ ).

#### *Heterochromatin Distribution in the Spinal Cord of PND 21 Mice*

Because the spinal cord develops earlier than the corpus callosum, I posited that heterochromatin distribution would show a greater difference between genotypes in spinal cord oligodendrocytes of PND 21 mice. No significant difference in ratios of total heterochromatin to total nuclear area was observed in oligodendrocytes of the spinal cord of PND 21 *LMNA* KO compared to oligodendrocytes from WT mice (Figure 3.2). Ten spinal cord oligodendrocytes per mouse were analyzed. WT mice had an average heterochromatin to nuclear area ratio of  $0.405 \pm 0.015$  ( $n=5$ ), while KO mice had a mean of  $0.388 \pm 0.025$  ( $n=5$ ) (t test  $p = 0.24$ ). Additionally, no difference between the percentage of heterochromatin localized near the inside periphery of the nuclear envelope to nuclear area was observed, with a WT peripheral heterochromatin to nuclear area mean of  $0.195 \pm 0.035$ , and a KO peripheral heterochromatin to nuclear area mean of  $0.189 \pm 0.029$  (t test  $p = 0.76$ ). There was also no significant difference in mean ratio of peripheral heterochromatin to total heterochromatin, WT mean of  $0.443 \pm 0.076$  and KO mean of  $0.470 \pm 0.057$  (t test  $p = 0.55$ ).

The *LMNA* gene is not specifically expressed in oligodendrocytes in the CNS. Therefore to determine if heterochromatin of other cell types was altered in the *LMNA* KO mice, heterochromatin ratios were also analyzed for spinal cord ventral horn motor neurons. No difference in ratios of total heterochromatin in the neuron nucleus was observed, with a WT mean of  $0.422 \pm 0.067$  ( $n=5$ ) and a KO mean of  $0.398 \pm 0.025$  ( $n=5$ ) (t test  $p = 0.48$ ) (Figure

3.3). Since no difference in the percent of heterochromatin was observed between genotypes for the motor neurons and since no significant difference was observed with regard to heterochromatin distribution in the oligodendrocytes in the spinal cord of PND 21 mice, further analysis of the peripheral heterochromatin ratios was not conducted for the PND 21 neurons.

### **Mean myelin thickness did not differ between WT and *LMNA* KO at PND 21 in either the corpus callosum or spinal cord**

To determine if the *LMNA* gene plays a role in myelination, g-ratios were calculated as a measure of myelin thickness, relative to the axon caliber.

G- ratios from the corpus callosum were calculated and plotted in a scatter plot with g-ratio on the y-axis and axon caliber in  $\mu\text{m}$  on the x-axis (Figure 3.4). Qualitative analysis revealed an overlap of the populations of g-ratios for both WT and *LMNA* KO. A Student's t test was performed to compare the means of g-ratios between WT, with a mean of  $0.768 \pm 0.00787$  ( $n = 3$ ), and *LMNA* KO, with a mean of  $0.772 \pm 0.0137$  ( $n = 3$ ), and no significant difference was observed ( $p = 0.827$ ). G ratios from the spinal cord were measured and plotted in a scatter plot with G ratio on the y-axis and axon caliber in  $\mu\text{m}$  on the x- axis (Figure 3.5). Qualitative analysis revealed an overlap of the populations of g-ratios for both WT and *LMNA* KO. Average g ratios between WT and *LMNA* KO were compared using a Student's t test. G ratios in the spinal cord of WT PND 21 mice had a mean of  $0.796 \pm 0.00677$  ( $n = 5$ ), with *LMNA* KO having a mean of  $0.807 \pm 0.00881$  ( $n = 5$ ) ( $p = 0.359$ ).

### **No difference in ratios of oligodendrocyte nuclear area to cytoplasm area was observed between WT and *LMNA* KO at PND 21**

Because our laboratory has previously shown that the oligodendrocyte cytoplasm area reduces with differentiation (Shroff and Dupree, unpublished data), ratios of nuclear area to cytoplasm area were analyzed as an assessment of oligodendrocyte maturity. No significant differences between WT and KO animals were seen at PND 21 in the oligodendrocytes of either the spinal cord or corpus callosum (Figure 3.6). In the spinal cord, PND 21 WT oligodendrocytes had a mean nucleus to cytoplasm ratio of  $0.592 \pm 0.027$  ( $n = 5$ ), and *LMNA* KO oligodendrocytes had a mean of  $0.582 \pm 0.027$  ( $n = 5$ ) ( $p = 0.806$ ). In the corpus callosum, WT oligodendrocytes of PND 21 animals had a mean nucleus to cytoplasm ratio of  $0.524 \pm 0.020$  ( $n = 4$ ), and KO had a mean of  $0.515 \pm 0.037$  ( $n = 4$ ) ( $p = 0.850$ ).

### ***LMNA* plays a role in heterochromatin organization in PND 35 mice**

No difference in heterochromatin organization was observed in *LMNA* KO mice as compared to WT mice at PND 21. Because *LMNA* expression increases with maturity, I next analyzed the *LMNA* KO mice at an older age. Based on published (Zhang et al., 2013) and unpublished (Hernandez and Casaccia, personal communication) observations, the *LMNA* KO mice die by 6 – 8 weeks of age. In our group's hands, PND 35 was the oldest age that could consistently be achieved for the *LMNA* KO mice; therefore, PND 35 was chosen for the “aged” analysis.

*LMNA regulates heterochromatin organization in corpus callosum oligodendrocytes of PND 35 mice*

Heterochromatin analysis was performed on ten oligodendrocytes per animal of both WT and *LMNA* KO PND 35 mice (Figure 3.7). No difference was observed in total heterochromatin to nuclear area ratios in *LMNA* KO (mean  $0.381 \pm 0.0123$ ,  $n = 4$ ) compared with WT (mean  $0.410 \pm 0.0148$ ,  $n = 4$ ) mice (t test  $p = 0.182$ ). When ratios of peripheral heterochromatin to nuclear area of corpus callosum oligodendrocytes were analyzed, significantly lower ratios were observed in the KO (mean  $0.204 \pm 0.00982$ ) compared against the WT (mean of  $0.258 \pm 0.00471$ ) (t test  $p < 0.01$ ). Additionally, lower ratios of peripheral heterochromatin to total heterochromatin were seen in the KO (mean  $0.534 \pm 0.0083$ ) compared with WT (mean  $0.627 \pm 0.017$ ) oligodendrocytes in the corpus callosum of PND 35 mice (t test  $p < 0.01$ ).

As a control for general effects of *LMNA* on heterochromatin distribution, cortical neurons from layers V and VI were also analyzed for heterochromatin ratios, with ten neurons from each animal for each genotype used for analysis (Figure 3.8). Consistent with all analyses, total heterochromatin to nuclear area ratios did not differ between the KO (mean  $0.217 \pm 0.030$ ,  $n = 3$ ) and WT (mean  $0.176 \pm 0.022$ ,  $n = 3$ ) (t test  $p = 0.332$ ) cortical neurons. Additionally, there was no significant difference in ratios of peripheral heterochromatin to total nuclear area between these cells in KO (mean  $0.0713 \pm 0.011$ ) and WT (mean  $0.0615 \pm 0.007$ ) (t test  $p = 0.519$ ). No differences were observed when comparing ratios of peripheral heterochromatin to total heterochromatin between KO (mean  $0.321 \pm 0.017$ ) and WT cortical neurons (mean  $0.362 \pm 0.011$ ) (t test  $p = 0.125$ ).

### *No Difference in Heterochromatin Distribution in the Optic Nerve of PND 35 LMNA KO Mice*

Since heterochromatin differences were observed in the oligodendrocytes from the corpus callosum in the PND35 mice, I conducted a similar analysis in the optic nerve to determine if this observed difference was regionally restricted in the CNS. (Figure 3.9). Ten oligodendrocytes per animal were analyzed for this region. No significant differences were seen in heterochromatin area to nuclear area ratios between oligodendrocytes in the optic nerve of PND 35 WT (mean of  $0.419 \pm 0.0193$ ,  $n = 4$ ) and *LMNA* KO (mean of  $0.406 \pm 0.0126$ ,  $n = 4$ ) mice ( $p = 0.609$ ). Peripheral heterochromatin area to nuclear area analyses were also not statistically significant, with WT oligodendrocytes having a mean of  $0.239 \pm 0.0114$ , and KO oligodendrocytes with a mean of  $0.221 \pm 0.0213$  ( $p = 0.494$ ). Additionally, peripheral heterochromatin area to total heterochromatin area ratios of oligodendrocytes from the optic nerve of WT (mean  $0.570 \pm 0.0102$ ) and KO (mean  $0.538 \pm 0.0376$ ) mice were not significantly different ( $p = 0.468$ ). Since there are no neuronal cell bodies in the optic nerve, I conducted heterochromatin analyses on optic nerve astrocytes (Figure 3.10), using six cells per animal. No significant differences were observed between WT (mean of  $0.312 \pm 0.0162$ ,  $n = 3$ ) and KO (mean of  $0.319 \pm 0.0104$ ,  $n = 3$ ) astrocytes (t test  $p = 0.743$ ).

### *LMNA Plays a Role in Heterochromatin Organization in Spinal Cord Oligodendrocytes of PND 35 Mice*

Myelination proceeds in a rostral to caudal gradient (Foran and Peterson, 1992), therefore I proposed that the greatest impact of knocking out *LMNA* would be observed in the cervical

region of the spinal cord (Foran and Peterson, 1992; Jordan et al., 1989). Ten oligodendrocytes per animal for both WT and *LMNA* KO were imaged and analyzed. No significant differences were seen in the total heterochromatin area to nuclear area ratios in WT (mean of  $0.413 \pm 0.0137$ ,  $n = 5$ ) and *LMNA* KO (mean of  $0.377 \pm 0.0116$ ,  $n = 5$ ) (t test  $p = 0.0802$ ) (Figure 3.11). However, there was significant reduction in the ratio of peripheral heterochromatin to nuclear area in the KO (mean of  $0.150 \pm 0.00905$ ) as compared to the WT (mean of  $0.204 \pm 0.00925$ ) (t test  $p < 0.01$ ). Additionally, there was a lower ratio of peripheral heterochromatin to total heterochromatin in the KO (mean of  $0.398 \pm 0.0240$ ) compared with the WT (mean of  $0.490 \pm 0.0184$ ) (t test  $p < 0.05$ ).

However, similar results were not seen in ventral horn spinal cord motor neurons of PND 35 mice (Figure 3.12). Total heterochromatin area to nuclear area ratios were not different in PND 35 *LMNA* KO spinal cord neurons (mean  $0.202 \pm 0.0176$ ,  $n = 3$ ) compared to WT littermates (mean  $0.218 \pm 0.00135$ ,  $n = 3$ ) (t test  $p = 0.454$ ). Additionally, ratios of peripheral heterochromatin to total nuclear area were not significantly different between KO (mean  $0.0643 \pm 0.0113$ ) and WT (mean  $0.0672 \pm 0.00316$ ) spinal cord motor neurons (t test  $p = 0.829$ ). Peripheral heterochromatin to total heterochromatin ratios also showed no difference between KO (mean  $0.320 \pm 0.0184$ ) and WT (mean  $0.332 \pm 0.0122$ ) spinal cord ventral horn neurons (t test  $p = 0.630$ ).

**Myelin thickness is reduced in the absence of *LMNA* in a region specific manner at PND 35**

*Absence of LMNA Does Not Have an Effect on Myelin Thickness in the Corpus Callosum of PND 35 Mice*

G ratios of 100 myelinated axons per animal from the corpus callosum of both WT and *LMNA* KO mice were calculated and plotted on an XY scatter plot (Figure 3.13) When g ratios of myelinated axons in the corpus callosum of PND 35 mice were plotted on an XY scatter plot, the populations of WT and *LMNA* KO overlapped. A Student's t test was used to determine if the means of the g ratios between WT and KO mice were different, and no significant difference was found. The mean value for KO g ratios in the corpus callosum was  $0.828 \pm 0.00928$  (n = 3), compared with the mean of the WT mice, which was  $0.823 \pm 0.00844$  (n = 4) (t test p = 0.711). Therefore, no significant difference in myelin thickness was seen between WT and *LMNA* KO in the corpus callosum of PND 35 mice.

*LMNA Impacts Myelin Thickness in the Spinal Cord of PND 35 Mice*

G ratios of 100 myelinated axons per animal from the spinal cord of both WT and *LMNA* KO mice were calculated and plotted on an XY scatter plot (Figure 3.14). The population of g ratios for the KO was shifted upward from the WT. Average g ratios per animal were compared between WT and KO in a Student's t test. The mean g ratio of myelinated axons in the *LMNA* KO spinal cord was  $0.856 \pm 0.019$  (n = 3), which was significantly different from the mean of the WT, which was  $0.811 \pm 0.008$  (n=3) (t test p < 0.05) suggesting impaired myelin formation in the spinal cord of KO mice.

### **Ratios of Oligodendrocyte Nuclear Area to Cytoplasm Area are not altered in the absence of *LMNA* in PND 35 Mice**

To determine if the *LMNA* gene played a role in oligodendrocyte maturity and differentiation at PND 35, oligodendrocyte nucleus to cytoplasm area ratios were calculated. No significant difference in cytoplasm to nuclear ratios was observed between WT and KO animals at PND 35 in the oligodendrocytes from the corpus callosum, optic nerve, and spinal cord (Figure 3.15). In the corpus callosum, WT oligodendrocytes had a mean nucleus to cytoplasm ratio of  $0.564 \pm 0.013$  (n = 4), and *LMNA* KO oligodendrocytes of PND 35 animals had a mean of  $0.621 \pm 0.042$  (n = 3) (t test p = 0.303). In the optic nerve, WT oligodendrocytes had nucleus to cytoplasm ratio of  $0.556 \pm 0.018$  (n = 3), which was not significantly different from the mean nucleus to cytoplasm ratio of *LMNA* KO oligodendrocytes of  $0.539 \pm 0.012$  (n = 3) (t test p = 0.473). In the spinal cord, PND 35 WT oligodendrocytes had a mean of  $0.521 \pm 0.034$  (n=4), and KO oligodendrocytes had a mean nucleus to cytoplasm ratio of  $0.620 \pm 0.023$  (n =4) (t test p = 0.102).

### **Results Summary**

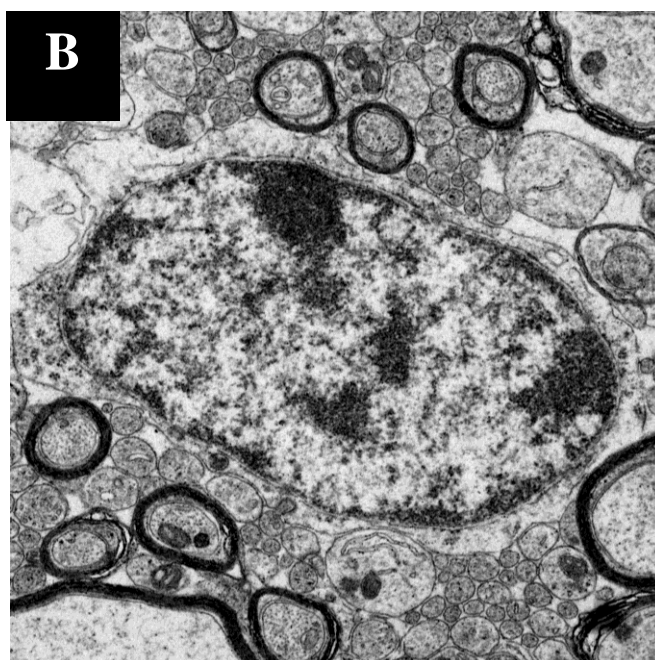
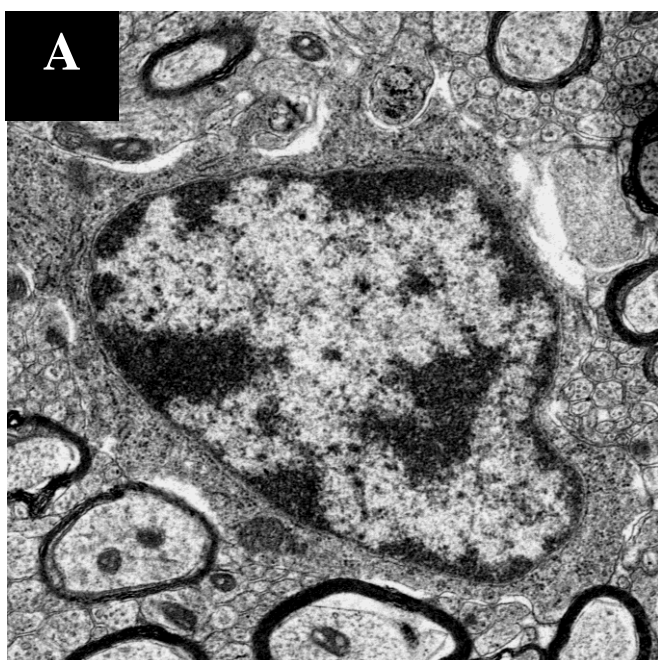
In summary, ratios of total heterochromatin to nuclear area, as well as peripheral heterochromatin to nuclear area and peripheral heterochromatin to total heterochromatin did not differ between oligodendrocytes in the corpus callosum or spinal cord of *LMNA* WT and KO mice at PND 21. G ratio linear regression analysis showed differing slopes between oligodendrocytes from the corpus callosum, but not spinal cord at PND 21, but g ratio means were not significantly different. No differences in nuclear area to cytoplasm area were observed

between oligodendrocytes from WT and KO mice in either the corpus callosum or spinal cord at PND 21.

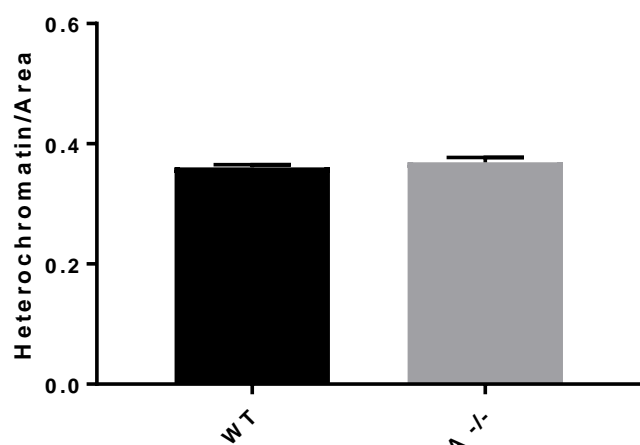
Although ratios of total heterochromatin to nuclear area did not differ between oligodendrocytes from WT and *LMNA* KO mice from the corpus callosum, spinal cord, or optic nerve of PND 35 mice, peripherally located heterochromatin was significantly reduced in the absence of A type lamins in the corpus callosum and spinal cord. G ratio values indicating thinner myelin were observed in spinal cord myelinated axons of *LMNA* KO mice at PND 35. No differences were observed in nuclear area to cytoplasm area ratios in any region analyzed at PND 35. Therefore, *LMNA* ablation resulted in no quantified global affect in myelination or oligodendrocyte chromatin organization at PND 21 in the CNS. In contrast, in the absence of A type lamins, peripheral heterochromatin was reduced and myelination was impaired in a region specific manner at PND 35.

**Figure 3.1. PND 21 corpus callosum oligodendrocytes show no difference in heterochromatin distribution.**

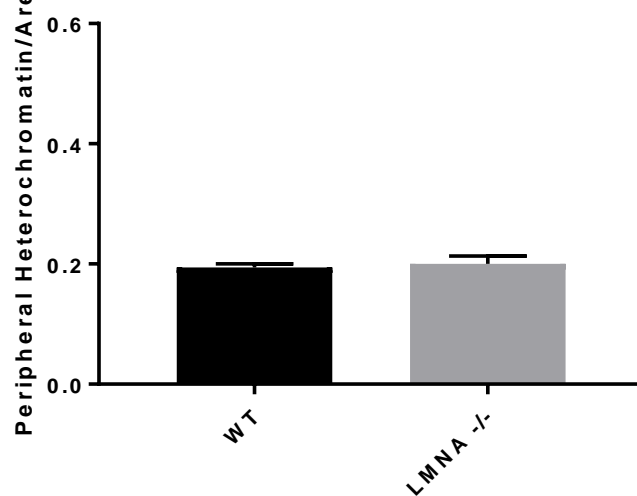
Ratios of total heterochromatin to nuclear area (C) did not differ significantly between oligodendrocytes in the corpus callosum from WT (A) and *LMNA* KO (B) mice in PND 21. Similarly, no significant difference in peripheral heterochromatin to total area (D) was observed between oligodendrocytes from WT and KO mice. Analysis of ratios of peripheral heterochromatin to total heterochromatin (E) also revealed no differences between genotypes.



**C.** Heterochromatin/Nuclear Area



**D.** Peripheral Heterochromatin/Area



**E.**

Peripheral/Total Heterochromatin

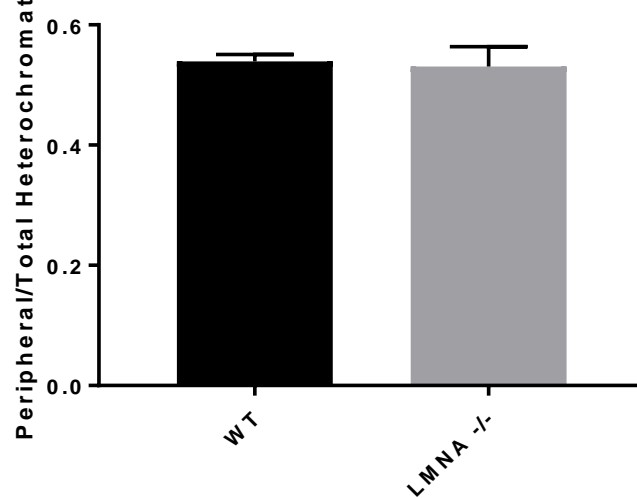
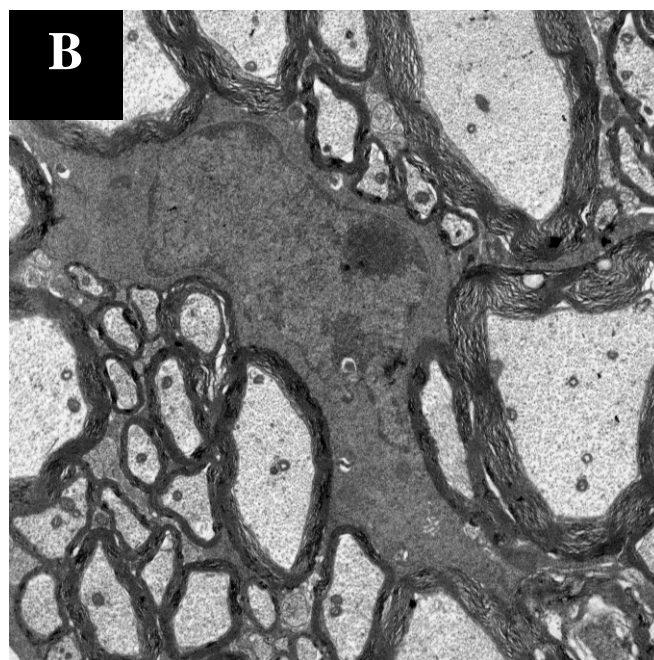
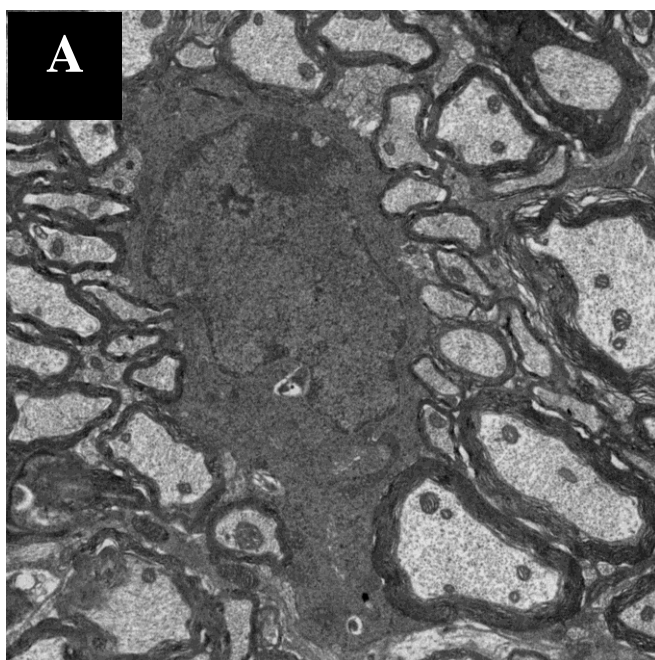
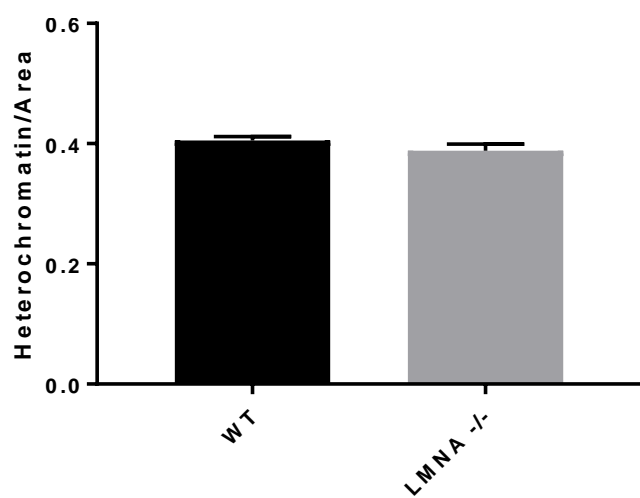


**Figure 3.2. PND 21 spinal cord oligodendrocytes show no difference in heterochromatin distribution.**

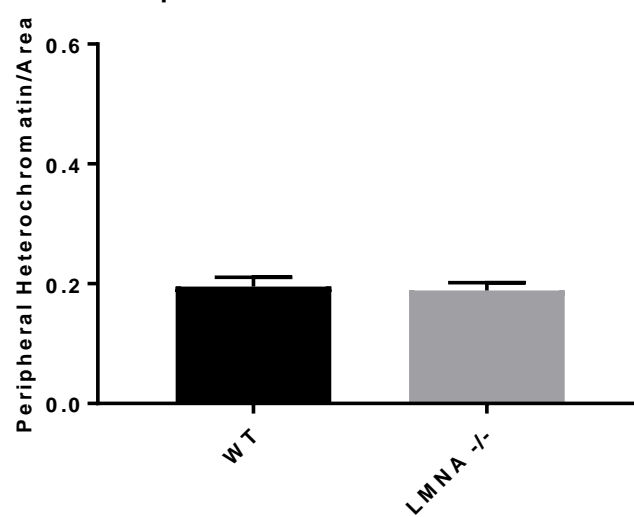
Ratios of total heterochromatin to nuclear area (C) did not differ significantly between oligodendrocytes from the spinal cord of WT (A) and *LMNA* KO (B) mice at PND 21. No significant difference in peripheral heterochromatin to total area (D) was observed between these cells from the WT and KO mice. Analysis of ratios of peripheral heterochromatin to total heterochromatin (E) also revealed no difference between genotypes.



**C.** Heterochromatin/Nuclear Area



**D.** Peripheral Heterochromatin/Area



**E.** Peripheral/Total Heterochromatin

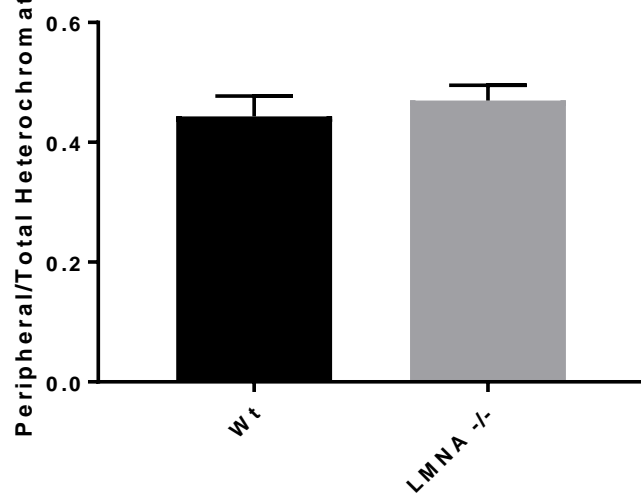
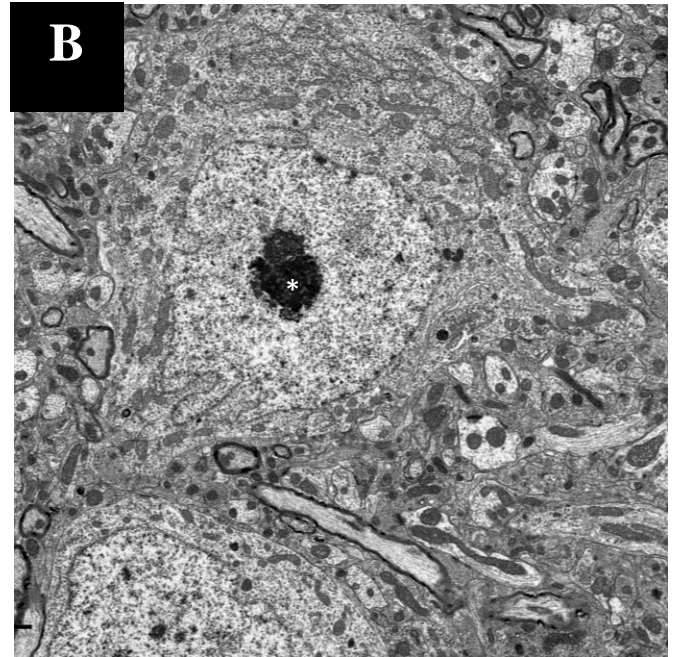
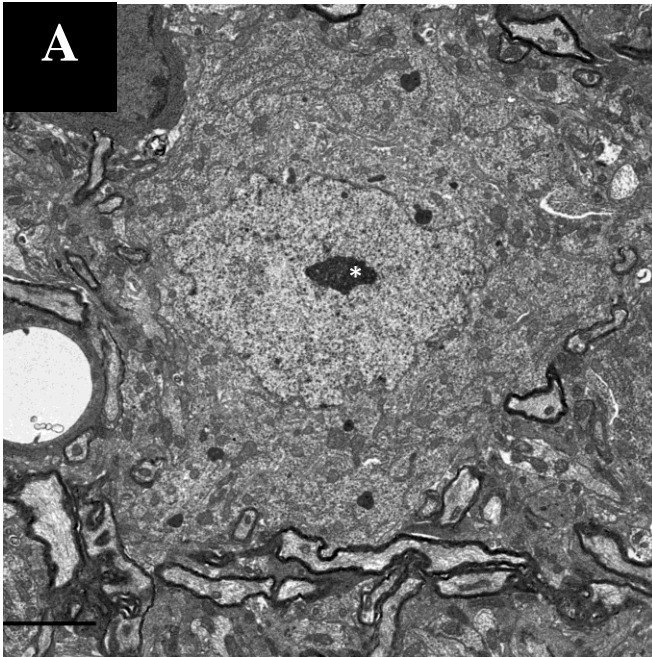


**Figure 3.3. No difference in heterochromatin of PND 21 Spinal Cord Ventral Horn Motor Neurons.**

Excluding the nucleolus (\*) of each cell, no difference in heterochromatin to nuclear area ratios (C) was observed between neurons of the spinal cord of WT (A) and LMNA KO (B) mice at PND 21.



**C.** Heterochromatin/Nuclear Area

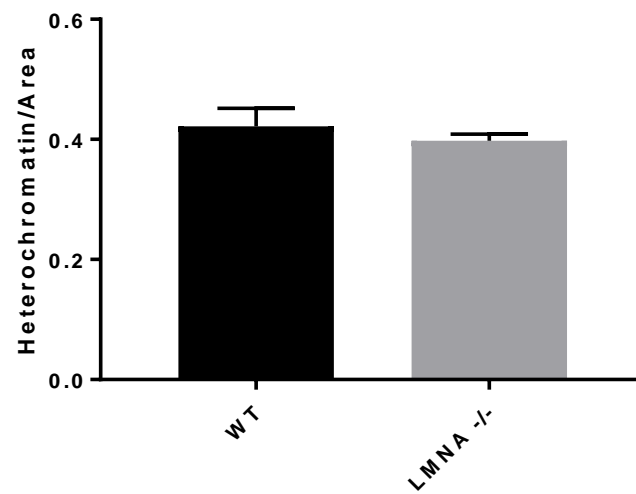


**Figure 3.4. G ratios of myelinated axons were not different in the corpus callosum at PND21**

Electron micrographs taken from the corpus callosum of WT (A) and LMNA KO (B) mice present myelinated axons with no difference in myelin g ratios with regard to the entire population as presented in a scatter plot (C) or based on mean g ratio value (D).

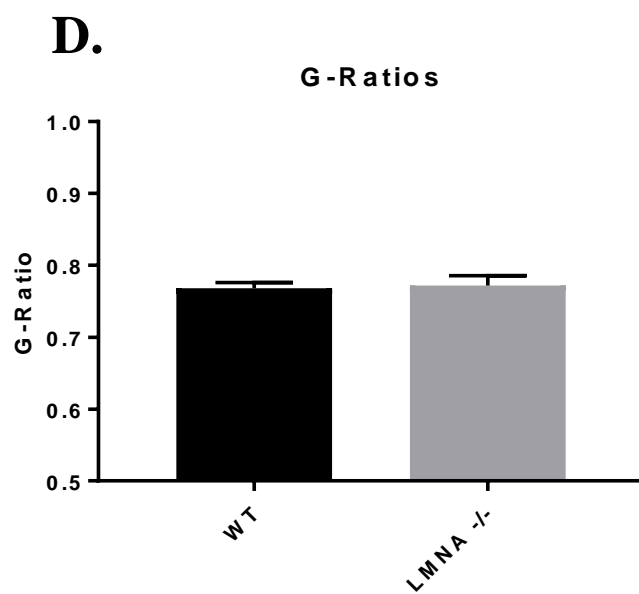
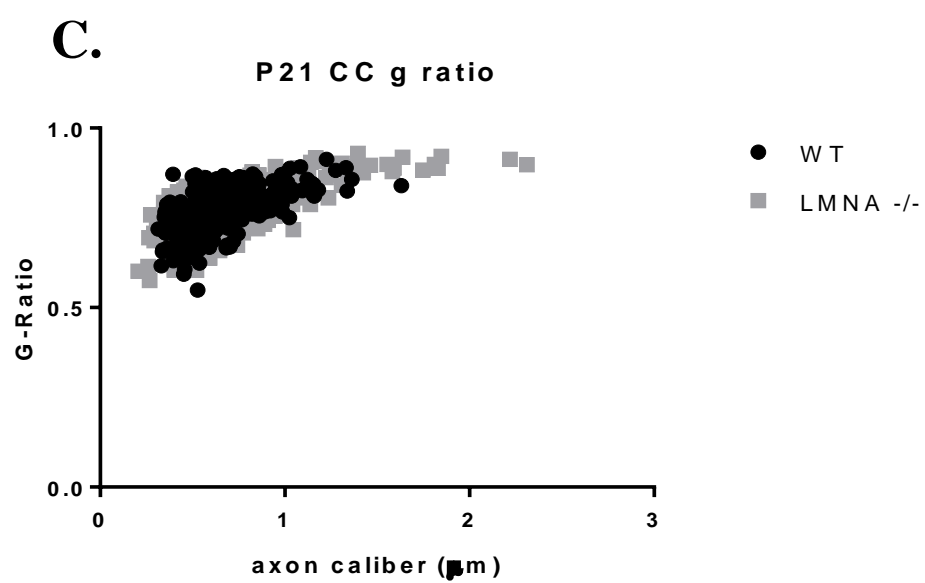
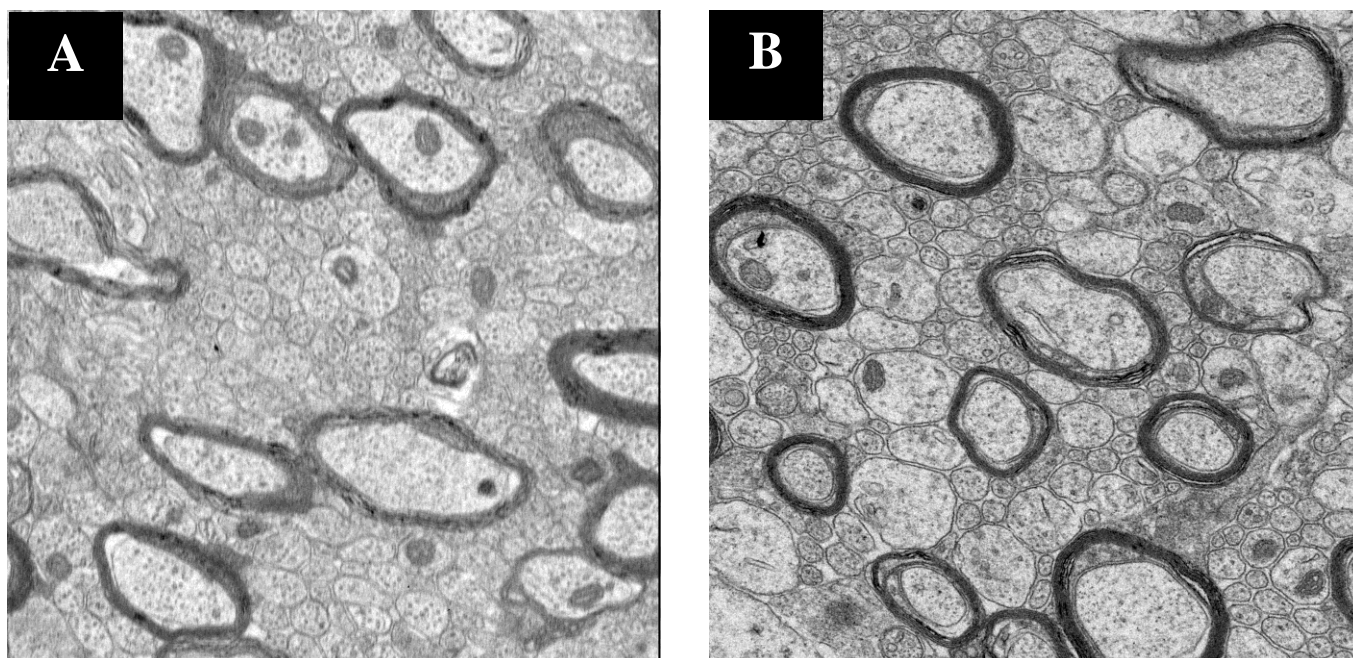


**Figure 3.5. PND 21 spinal cord myelinated axons show no difference in myelin thickness.**

Quantitative analysis of myelinated axons in the spinal cord of WT (A) and LMNA KO (B) mice revealed no difference in g ratios either by scatter plot analysis to compare g ratios versus axon caliber (C) or by g ratio means (D) .

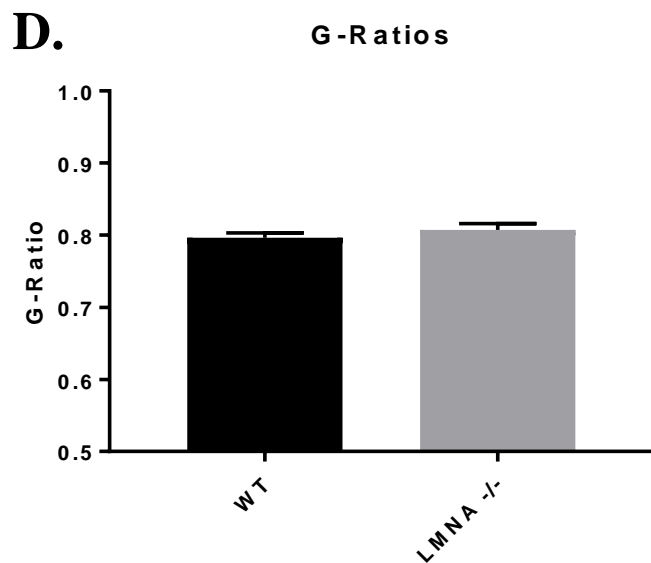
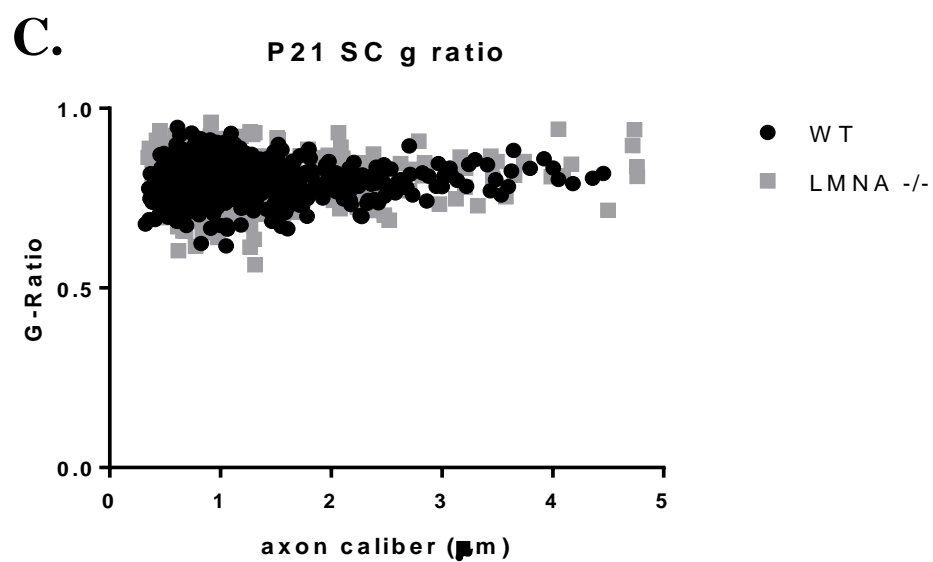
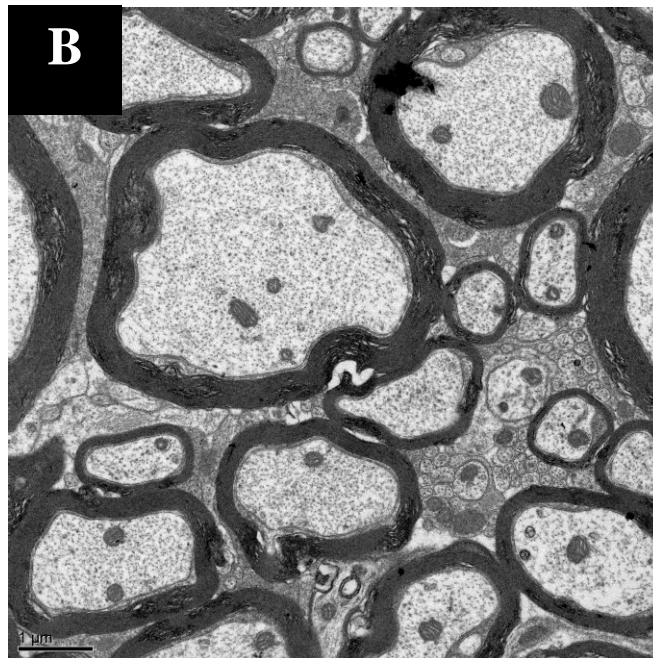
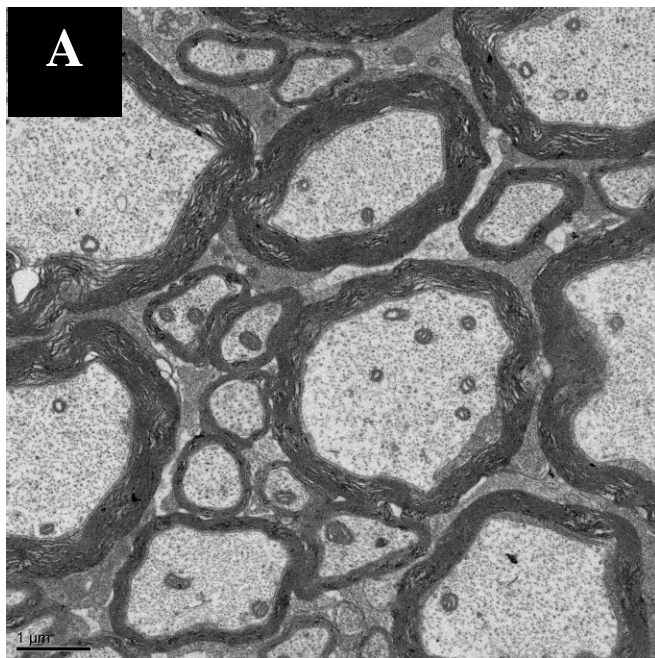
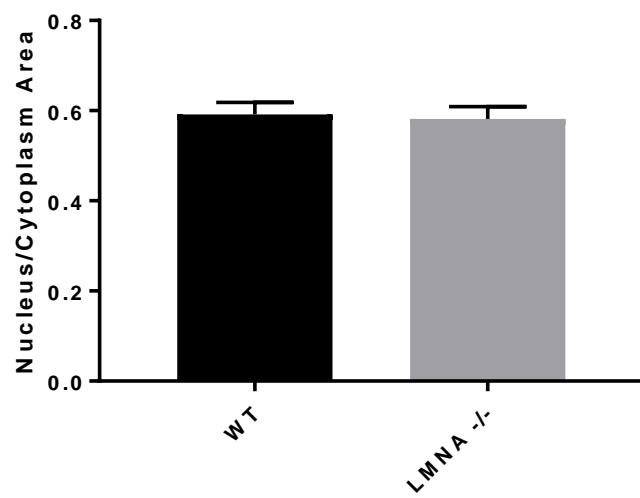


**Figure 3.6. Oligodendrocytes from the spinal cord or corpus callosum from WT and LMNA KO mice revealed no difference in nucleus to cytoplasm ratio at PND 21.**

The ratio of the nucleus to cytoplasm of oligodendrocytes has previously been used to assess oligodendrocyte maturity. Here, this ratio was not different for the oligodendrocytes from either the spinal cord (A) or the corpus callosum (B) of the WT and LMNA KO mice.

**A.** SC Nucleus/Cytoplasm Area



**B.** CC Nucleus/Cytoplasm Area

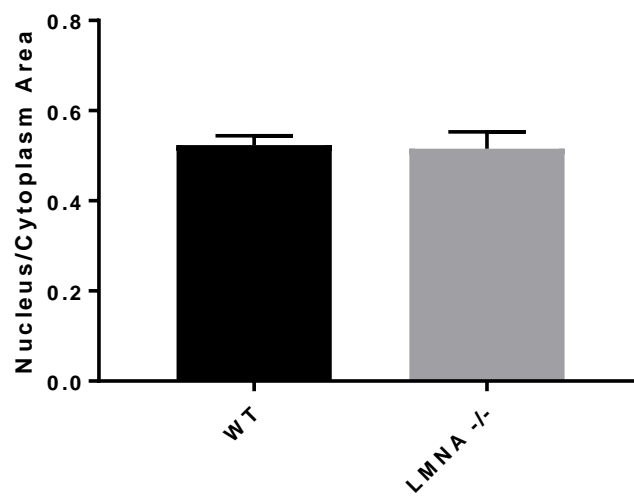
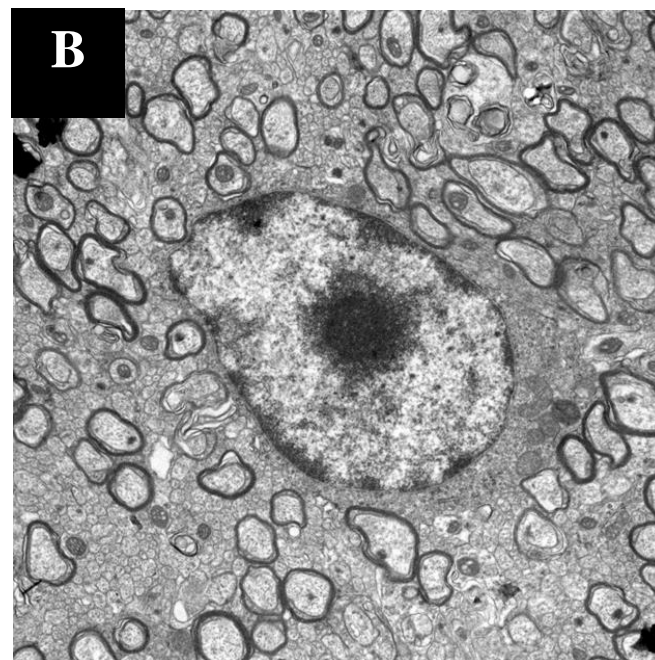
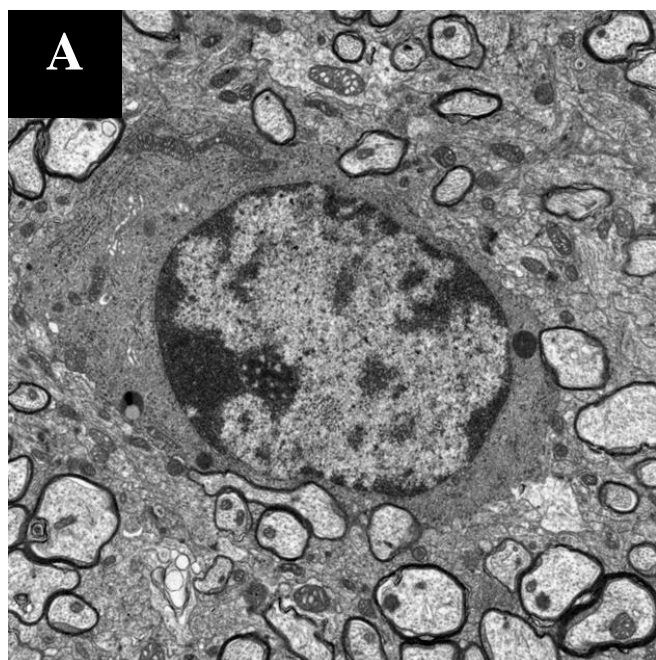
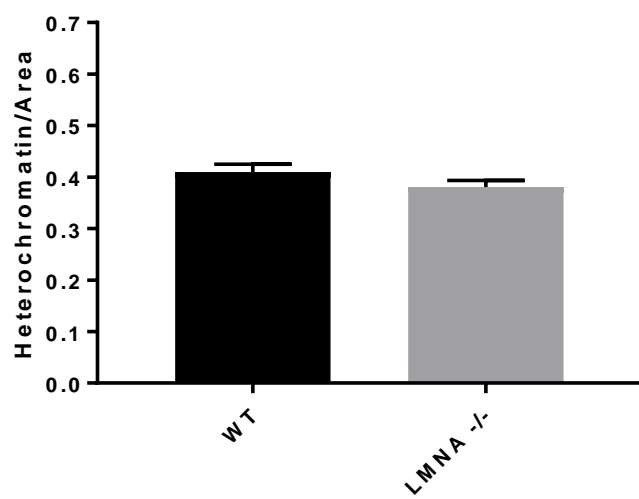


**Figure 3.7. Peripheral Heterochromatin was significantly reduced in the oligodendrocytes from the corpus callosum of PND 35 *LMNA* KO compared to WT mice.**

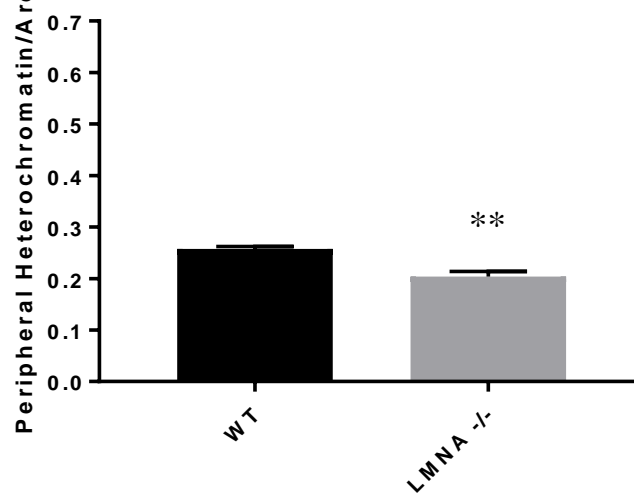
No difference in ratios of total heterochromatin to nuclear area between oligodendrocytes from WT (A) and *LMNA* KO (B) mice was observed in the corpus callosum at PND 35 (C). In contrast, ratios of peripheral heterochromatin to nuclear area (D) and peripheral heterochromatin to total heterochromatin (D) were significantly different between oligodendrocytes from the WT and *LMNA* KO mice.



**C.** Heterochromatin/Nuclear Area



**D.** Peripheral Heterochromatin/Area



**E.** Peripheral/Total Heterochromatin

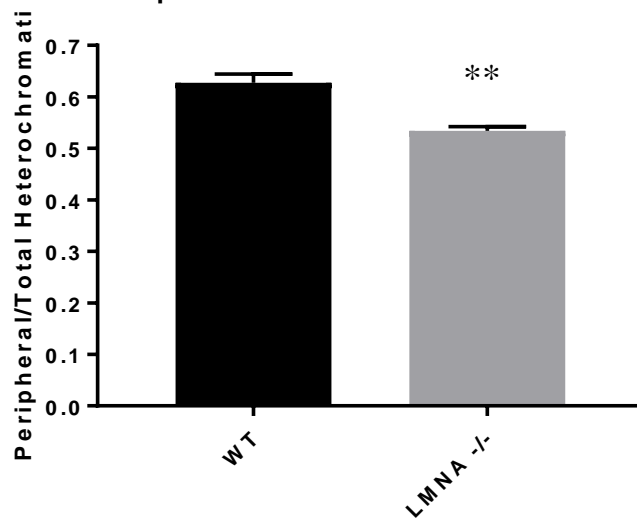
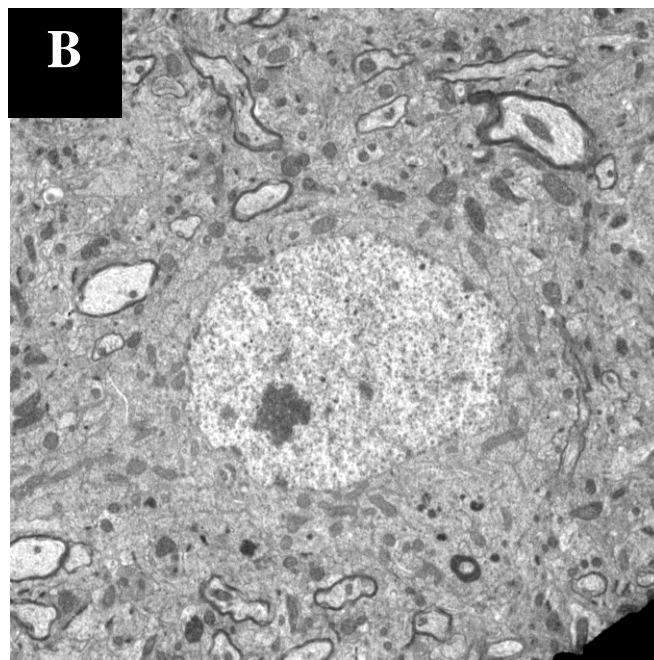
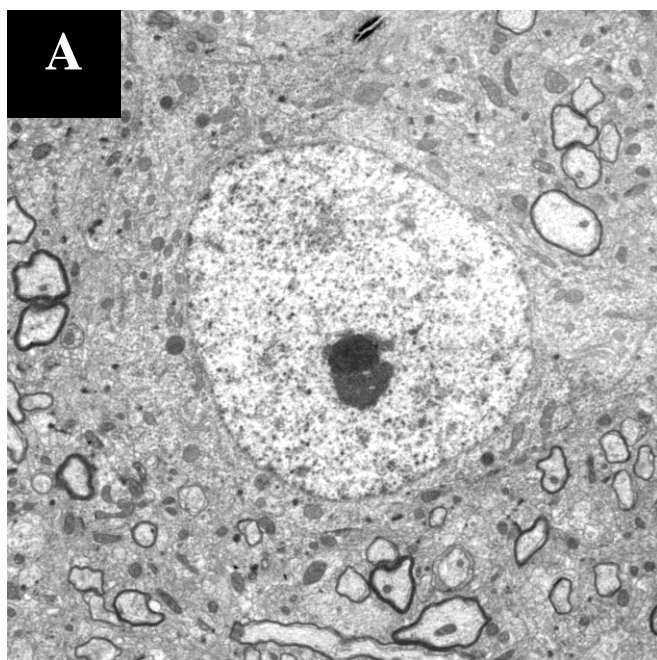
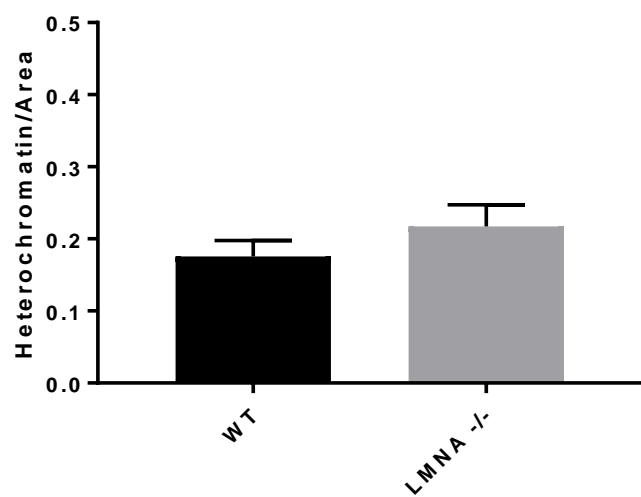


**Figure 3.8. PND 35 cortical neurons display no difference in heterochromatin distribution.**

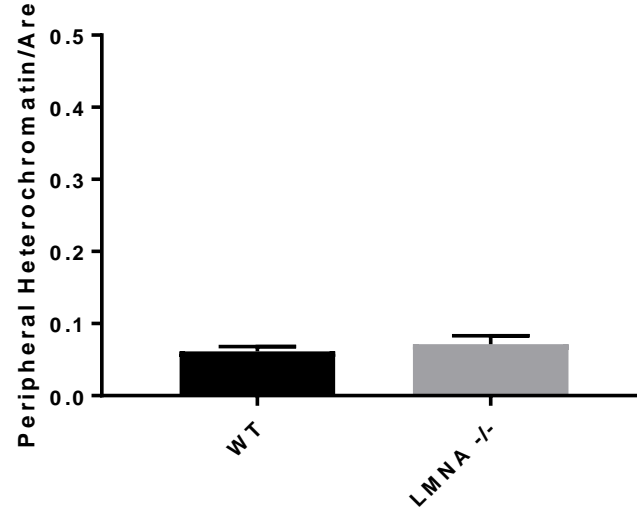
Cortical neurons from PND 35 WT (A) and *LMNA* KO (B) mice revealed no difference in the ratios of total heterochromatin to nuclear area (C) , peripheral heterochromatin to nuclear area (D), or peripheral heterochromatin to total heterochromatin (E).



**C.** Heterochromatin/Nuclear Area



**D.** Peripheral Heterochromatin/Area



**E.** Peripheral/Total Heterochromatin

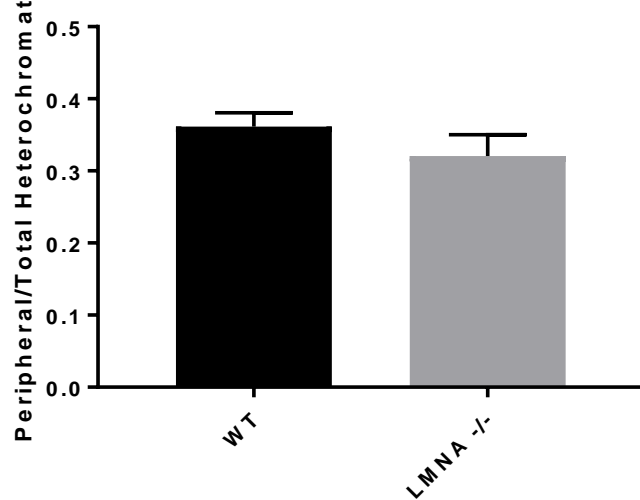
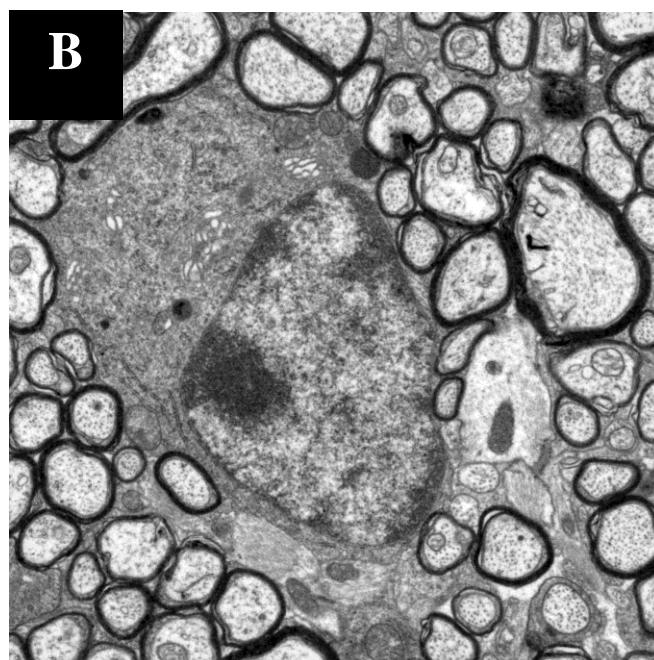
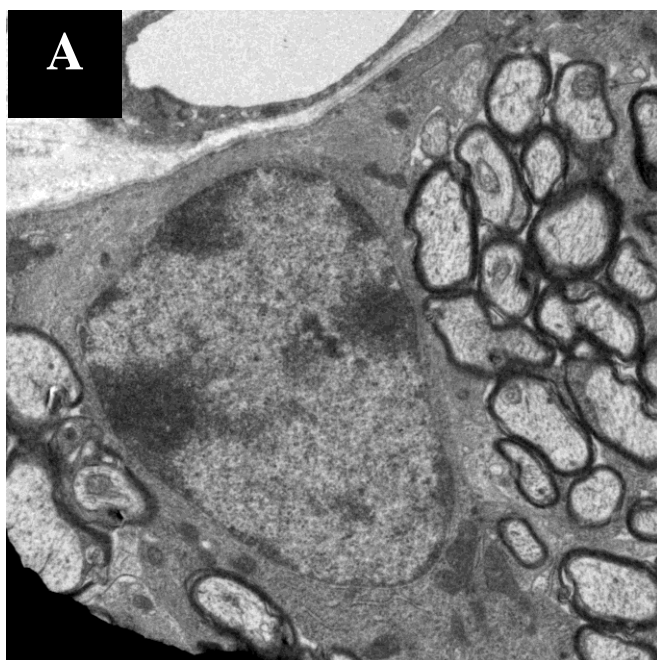
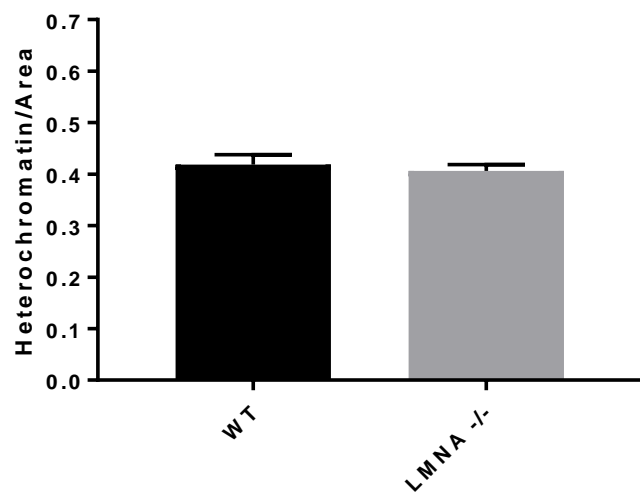


**Figure 3.9. PND 35 optic nerve oligodendrocytes show no difference in heterochromatin distribution.**

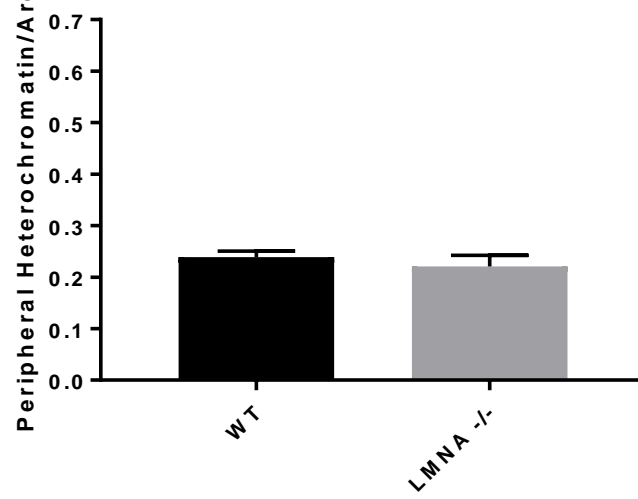
Oligodendrocytes from the optic nerves of PND 35 WT (A) and *LMNA* KO (B) mice revealed no difference in ratios of total heterochromatin to nuclear area (C) , peripheral heterochromatin to nuclear area (D), or peripheral heterochromatin to total heterochromatin (E).



**C.** Heterochromatin/Nuclear Area



**D.** Peripheral Heterochromatin/Area



**E.** Peripheral/Total Heterochromatin

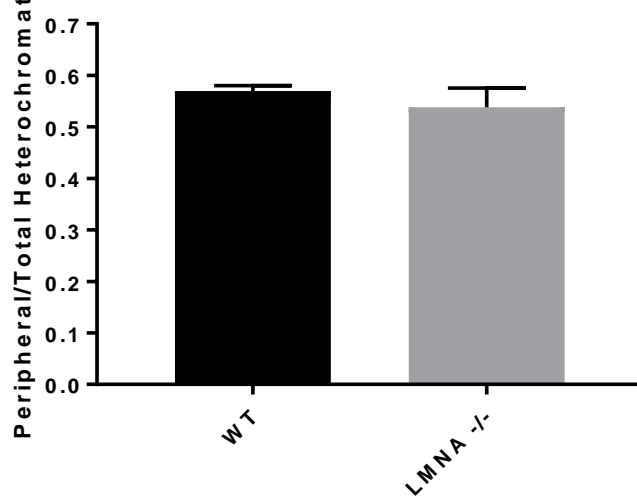
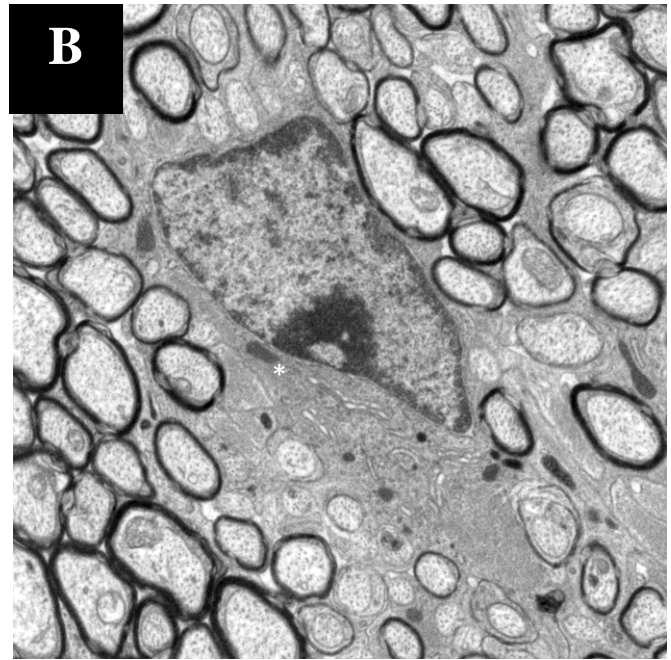
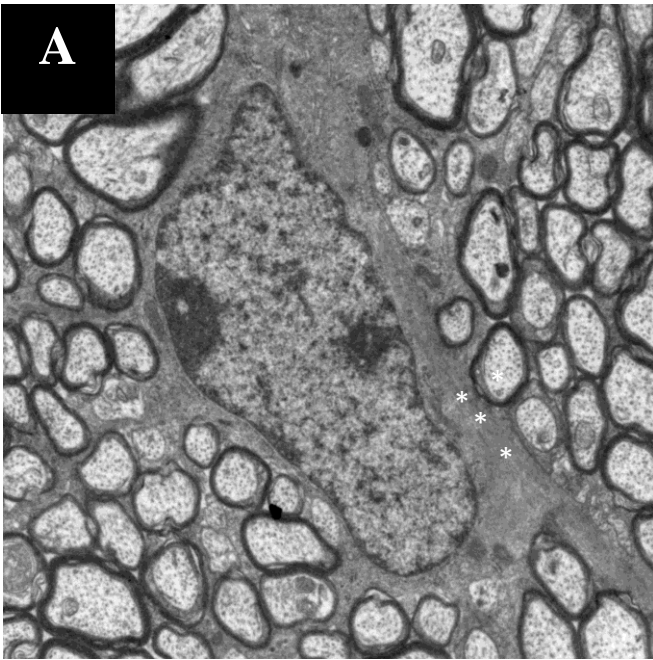


**Figure 3.10. No difference in heterochromatin of PND 35 Optic Nerve Astrocytes.**

Astrocytes from the optic nerves of PND 35 WT (A) and LMNA KO (B) mice revealed no difference in the ratio of heterochromatin to nuclear area. Astrocytes were identified by the presence of the intermediate filament protein glial fibrillary acidic protein (\*).



### C. Heterochromatin/Nuclear Area

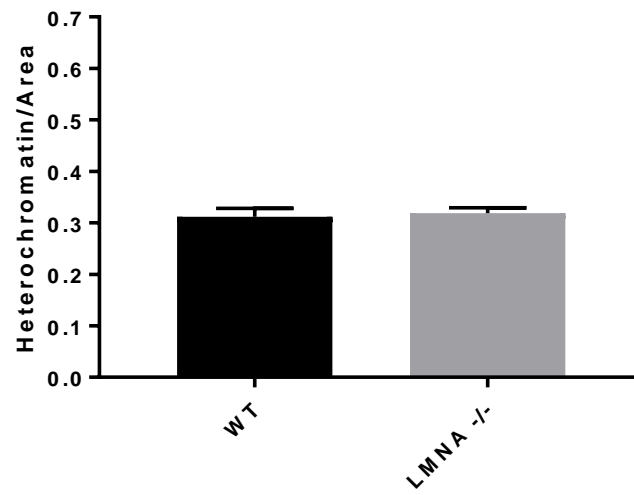
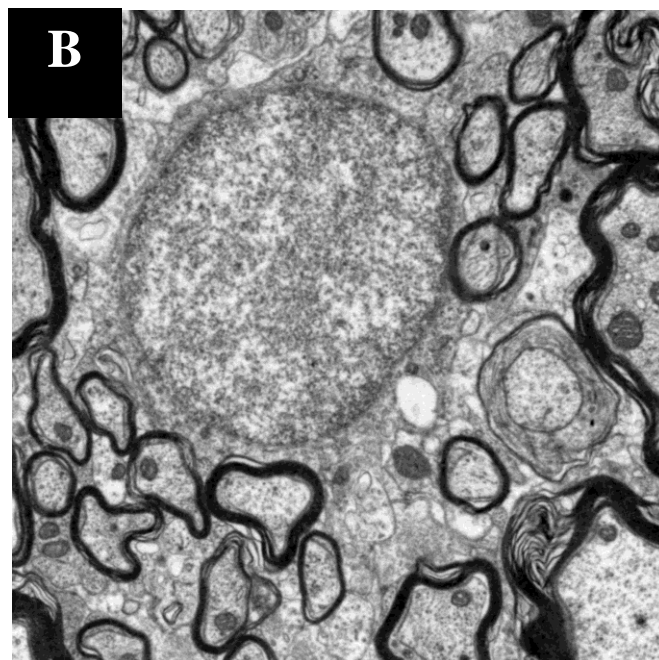
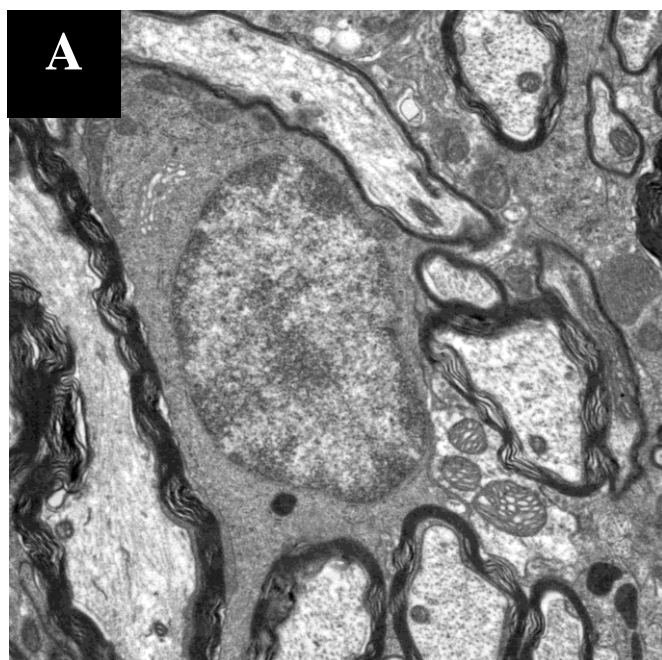
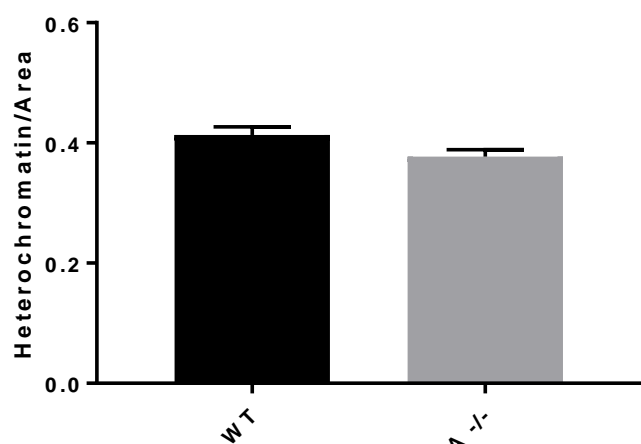


**Figure 3.11. Heterochromatin organization is altered in the spinal cord of PND 35 *LMNA* KO mice.**

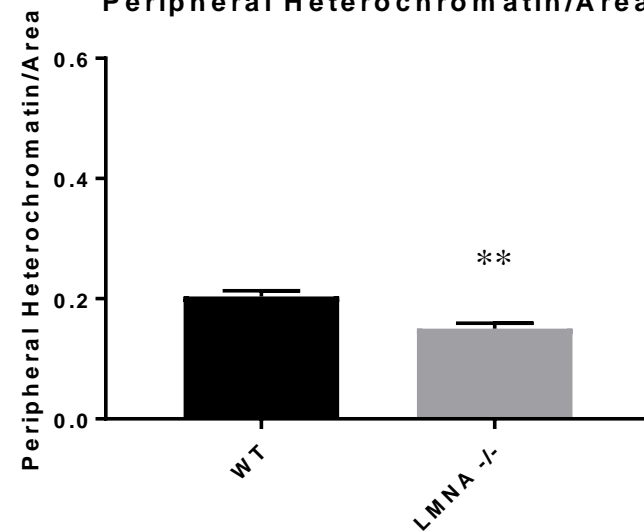
No difference between total heterochromatin area to nuclear area ratios was observed in spinal cord oligodendrocytes from PND 35 WT (A) and *LMNA* KO (B) mice (C). However, ratios of peripheral heterochromatin to total nuclear area were significantly reduced in the oligodendrocytes of *LMNA* KO mice (D). Additionally, ratios of peripheral heterochromatin to total heterochromatin were significantly lower in the *LMNA* KO oligodendrocytes (E).



**C.** Heterochromatin/Nuclear Area



**D.** Peripheral Heterochromatin/Area



**E.** Peripheral/Total Heterochromatin

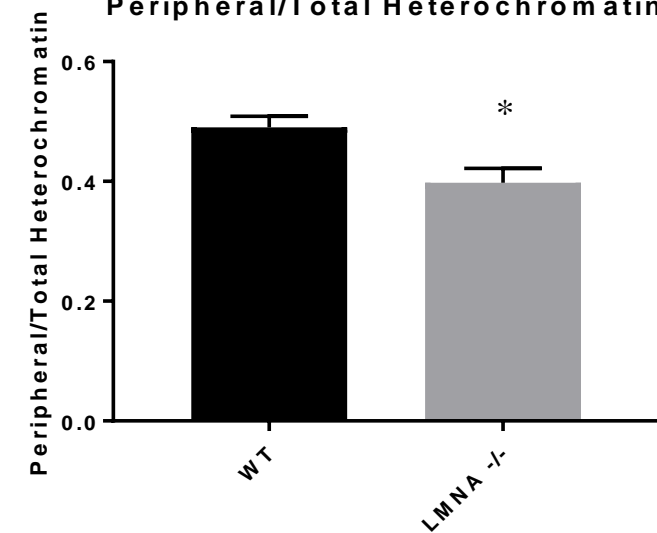
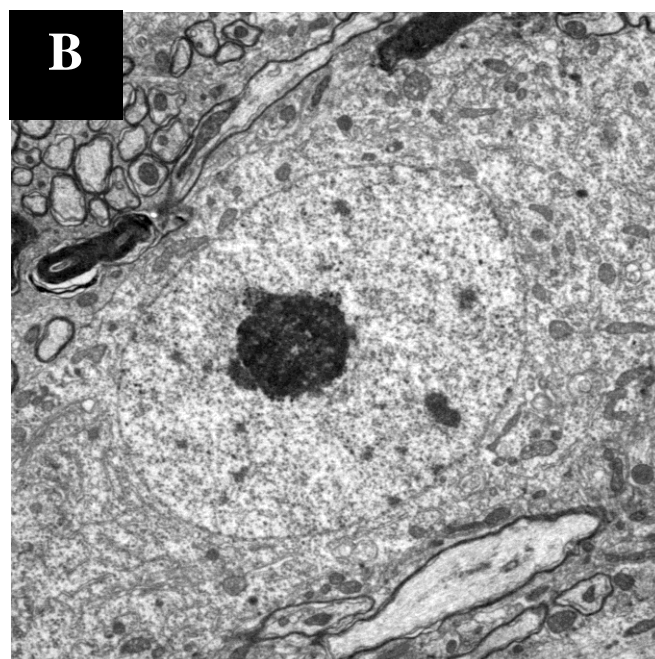
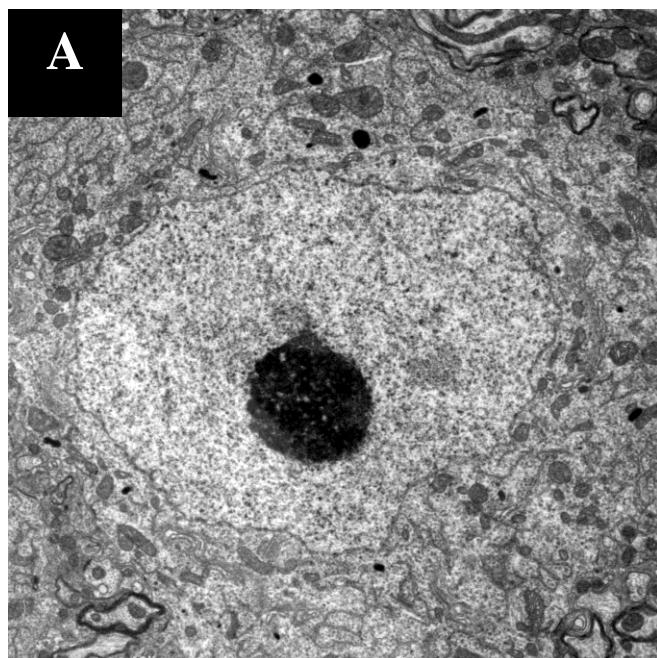
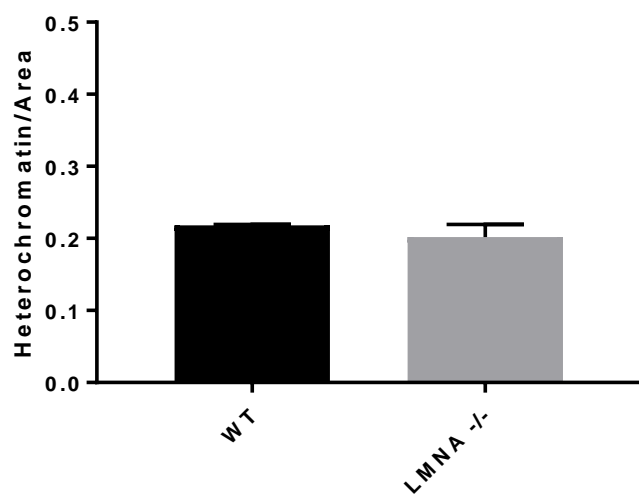


**Figure 3.12. PND 35 spinal cord neurons show no difference in heterochromatin distribution.**

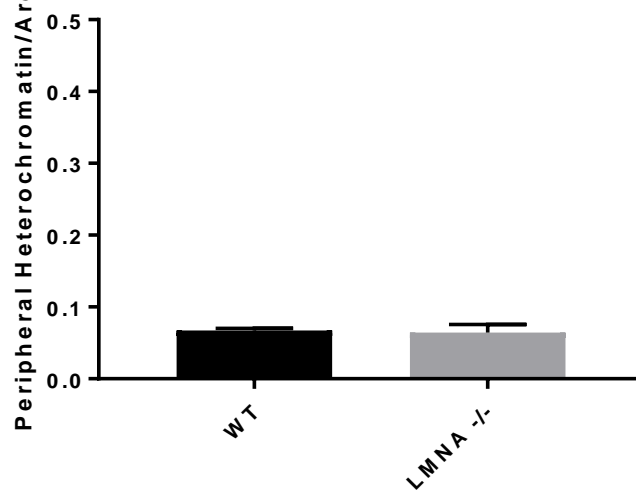
Spinal cord neurons from PND 35 WT (A) and LMNA KO (B) mice revealed no difference in the ratios of heterochromatin to nuclear area (C), peripheral heterochromatin to nuclear area (D), or peripheral heterochromatin to total heterochromatin (E).



**C.** Heterochromatin/Nuclear Area



**D.** Peripheral Heterochromatin/Area



**E.** Peripheral/Total Heterochromatin

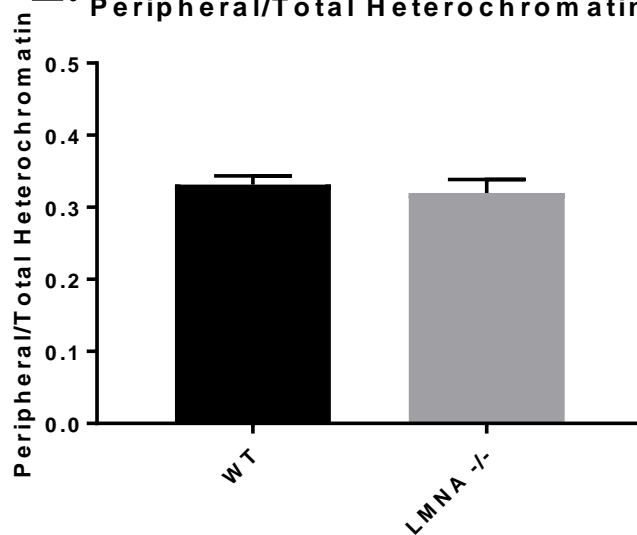


**Figure 3.13. G ratios of myelinated axons were not different in between genotypes in the corpus callosum at PND35**

Quantitative analysis of myelinated axons in the spinal cord of PND 35 WT (A) and LMNA KO (B) mice revealed no difference in g ratios either by scatter plot analysis to compare g ratios versus axon caliber (C) or by g ratio means (D) .

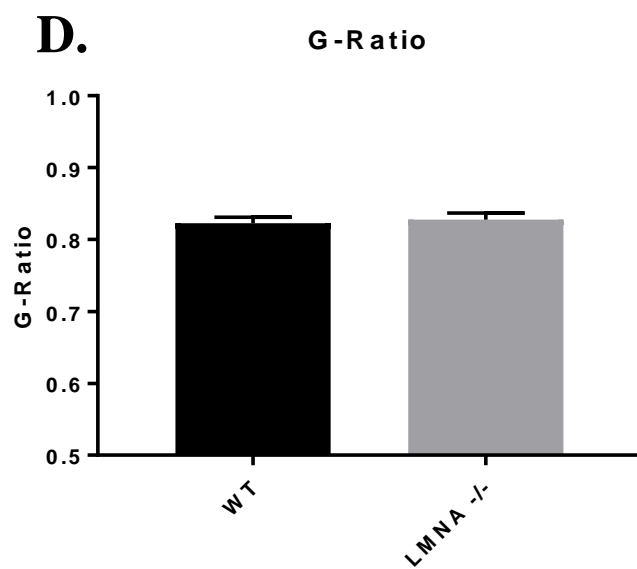
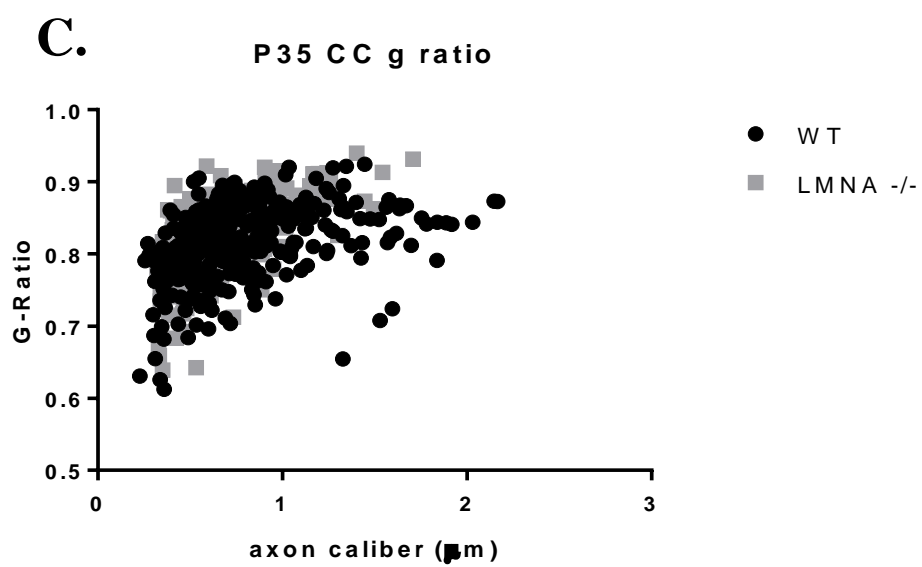
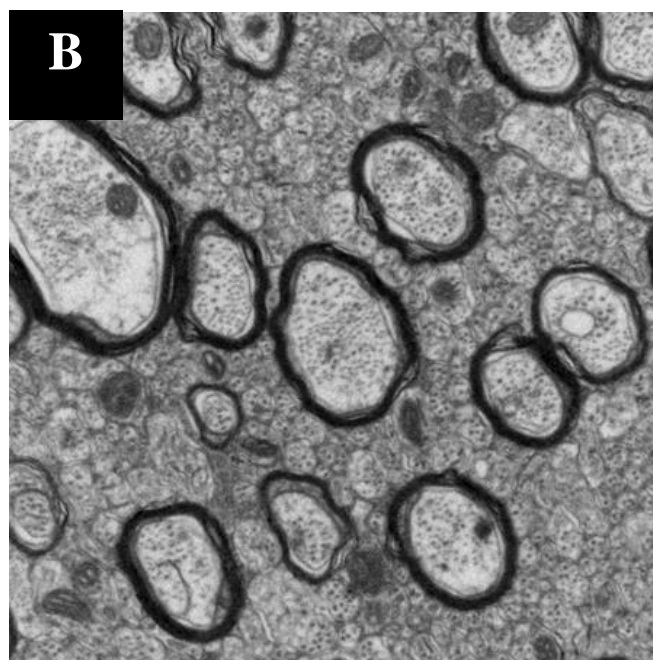
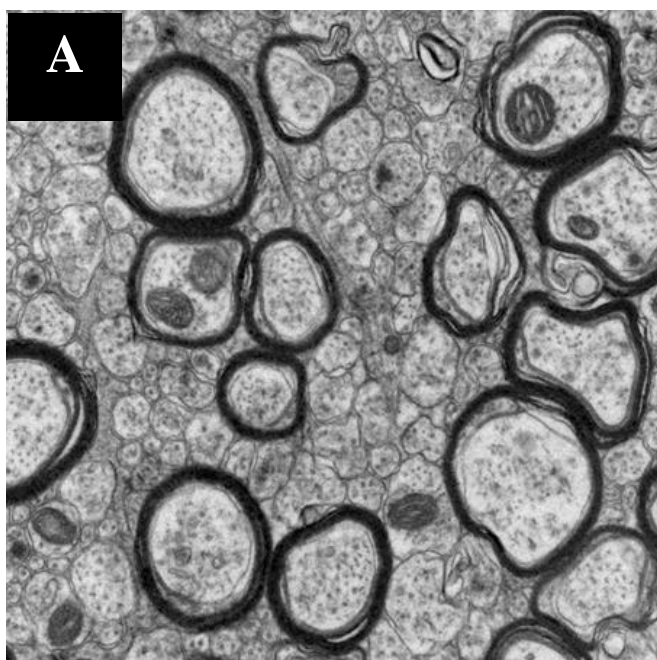


**Figure 3.14. G ratios of spinal cord myelinated axons were significantly thinner in the LMNA KO mice compared to the WT animals at PND35**

Quantitative analysis of myelinated axons in the spinal cord of PND 35 WT (A) and LMNA KO (B) mice revealed significantly greater mean g ratios in the KO animals (D) although the distribution of g ratios as assessed by a scatter plotter revealed no obvious difference between genotypes (C).

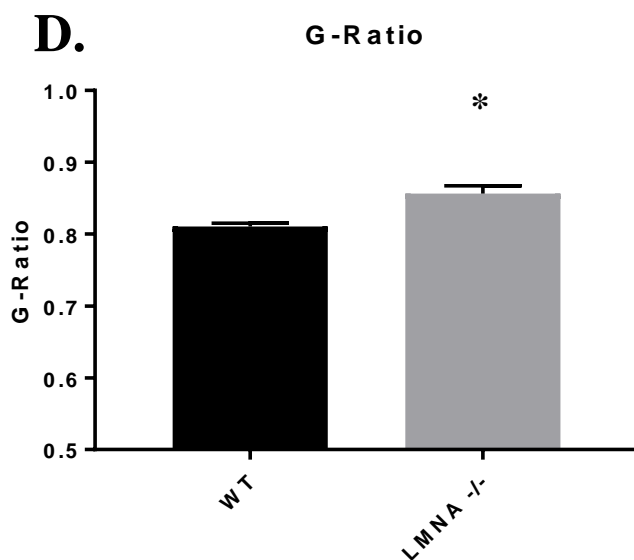
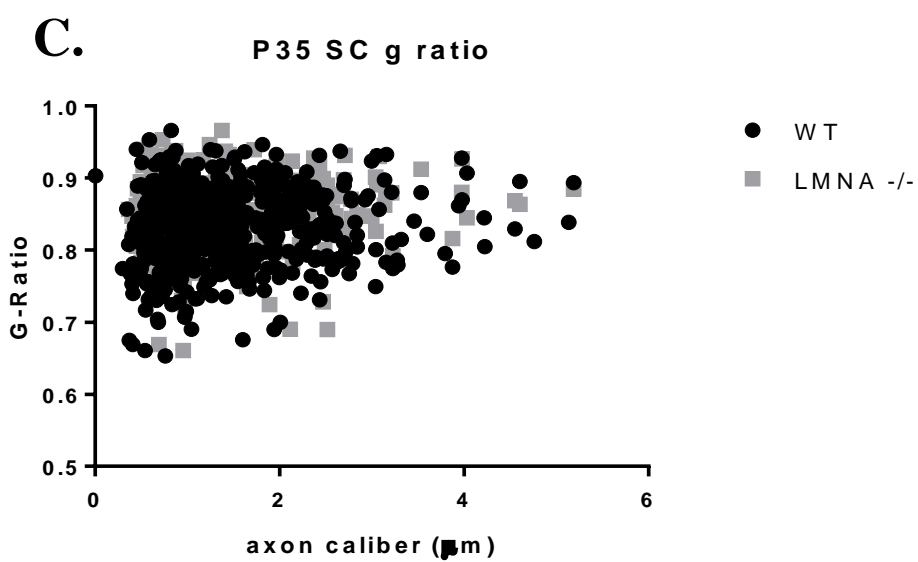
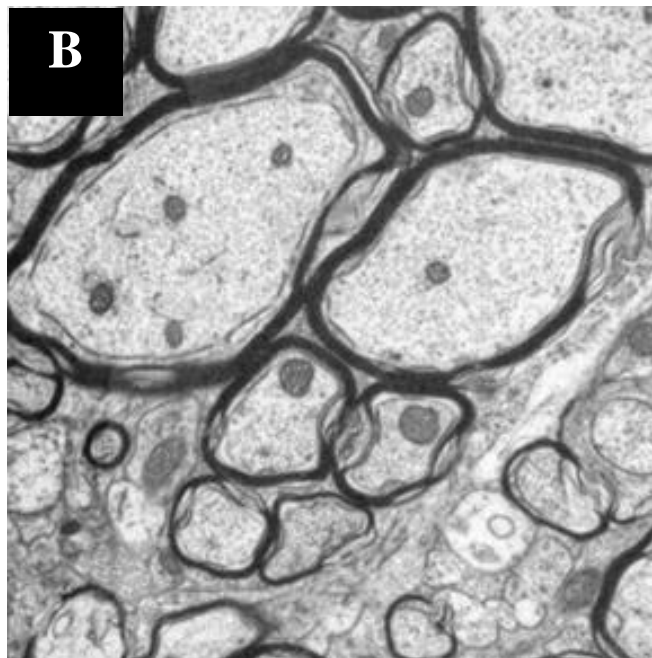
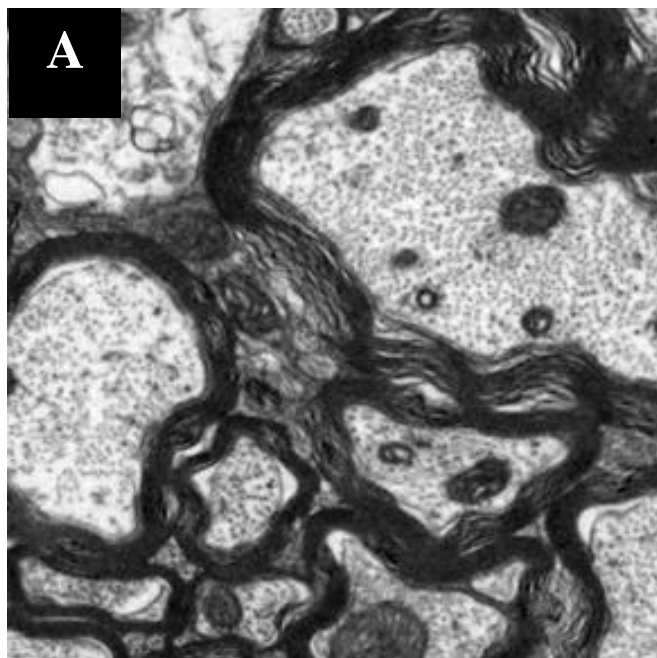
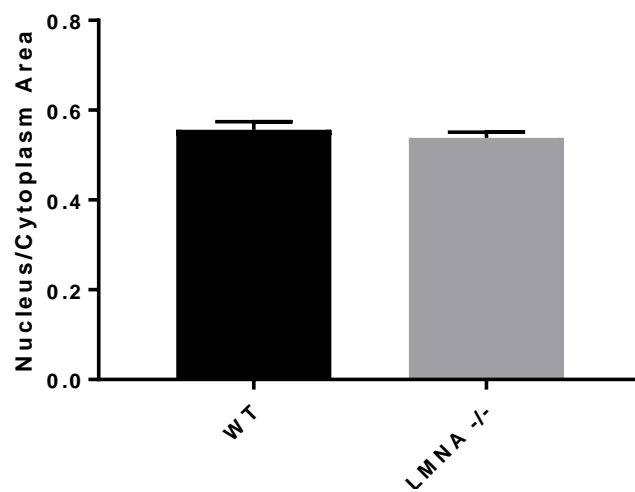


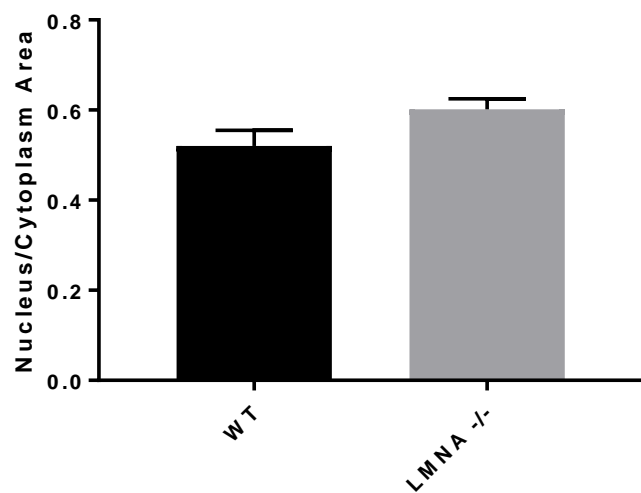
**Figure 3.15. Oligodendrocytes from the optic nerve, spinal cord or corpus callosum from WT and LMNA KO mice revealed no difference in nucleus to cytoplasm ratio at PND 35 mice.**

The ratio of the area of the nucleus to the cytoplasm was not different for the oligodendrocytes from the optic nerve (A), the spinal cord (B) or the corpus callosum (C) of WT and LMNA KO mice.

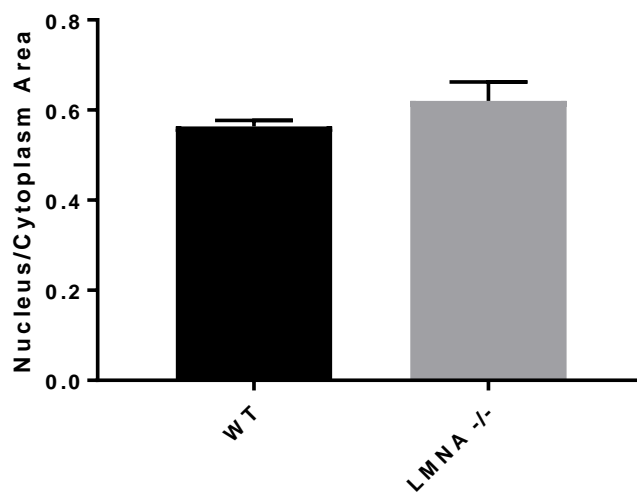
**A.** Optic Nucleus/Cytoplasm



**B.** Spinal Cord Nucleus/Cytoplasm



**C.** Corpus Callosum Nucleus/Cytoplasm



## DISCUSSION

Multiple sclerosis is a demyelinating disorder of the CNS that results in impaired motor, sensory and cognitive dysfunction (Ma et al., 2014). In order to develop novel remyelinating clinical strategies, it is imperative to elucidate mechanisms that regulate myelin formation. In this study, I postulated that the nuclear envelope proteins, lamins A and C, play a role in regulating oligodendrocyte development and myelin formation. The data gathered through electron microscopic analyses suggest that *LMNA* plays a temporal and spatial role in heterochromatin distribution in the oligodendrocyte nucleus and subsequently may regulate myelin thickness in the CNS. However, ratios of total heterochromatin to nuclear area did not differ significantly, suggesting *LMNA* does not impact heterochromatin formation itself. An effect of *LMNA* was not observed when nuclear area to cytoplasm area ratios were compared between WT and KO mice. No difference between *LMNA* KO and WT was seen in any analysis at PND 21, but differences in oligodendrocytes and myelination in certain CNS regions were observed by PND 35. Lamins A and C proteins are undetectable in the murine brain prior to PND 15 (Roeber et al., 1989). This suggests that there is a delay in the impact of A type lamins on oligodendrocytes and myelination. Ablation of *LMNA* affected peripheral heterochromatin in both the spinal cord and corpus callosum of PND 35 mice, but not in the optic nerve. Oligodendrocytes in the optic nerve are primarily a population of type I and II oligodendrocytes, which myelinate smaller caliber axons (Butt et al., 1994). Since larger caliber axons are myelinated first, with smaller caliber axons being myelinated after PND 20, it is possible that the effect of *LMNA* on optic nerve oligodendrocytes is not yet observable at PND 35 (Hildebrand et

al., 1993). However, the possibility remains that A type lamins play a different role in oligodendrocytes of the optic nerve, or that optic nerve oligodendrocytes have compensatory mechanisms not found in oligodendrocytes of the corpus callosum or spinal cord.

Because myelination proceeds in a rostral to caudal gradient beginning in the spinal cord (Foran and Peterson, 1992) the timeline of myelination is different between the spinal cord and corpus callosum, with the spinal cord reaching peak myelination at PND 20 and achieving peak myelination by PND 45 in the corpus callosum (Benjamins and Morell, 1978; Sturrock, 1980). Thinner myelin was observed in the spinal cord of *LMNA* KO mice at PND 35, but was not statistically significant in the corpus callosum (Figure 3.23). Potentially, A type lamins play distinct roles in myelination in the spinal cord and corpus callosum. However, it is possible that the impact of A type lamins on corpus callosum myelination is not yet identifiable at PND 35. Overall, this study presents novel findings for the role of A type lamins in a previously unstudied cell type.

### ***LMNA* affects heterchromatin architecture in the oligodendrocyte nucleus temporally and spatially**

The distribution and architecture of chromatin is a prominent factor in epigenetic regulation of gene expression (Bartova et al., 2008). Typically, transcriptionally active genes localize to the nuclear interior, while inactive genes are frequently targeted to heterochromatic regions of the nuclear periphery as a method of silencing gene expression, as the compact nature of heterochromatin makes it generally inaccessible to DNA binding factors (Heitz, 1928; Cockell

and Gasser, 1999; Nielsen et al., 2002; Copray et al., 2009). Because of this, it was of interest to determine if the loss of *LMNA*, a gene encoding lamins A and C intermediate filaments that associate with peripherally located heterochromatin, altered the distribution of heterochromatin in the oligodendrocyte nucleus (Nikolova et al., 2004).

It was hypothesized that, in the absence of A type lamins, peripheral heterochromatin would be reduced. Consistent with the findings of Harr et al. (2015), the association of heterochromatin with the nuclear periphery was affected, with heterochromatin localizing to the nuclear interior, creating an inverted distribution. However, this difference was only observed in the older mice as no difference in heterochromatin distribution was observed between WT and *LMNA* KO at PND 21. This is likely due to the early time point, as lamins A and C proteins are not detectable until PND 15 (Roeber et al., 1989). Of the time points studied, the effects of *LMNA* on peripheral heterochromatin were only seen in PND 35 animals, and restricted to oligodendrocytes of the corpus callosum and spinal cord. Compensatory mechanisms for *LMNA* ablation have been identified, including functions of B type lamins (Galiova et al., 2008; Imai et al., 1997). Oligodendrocytes of the optic nerve may have compensatory mechanisms not present in those of the corpus callosum and spinal cord, or it could be that differences in heterochromatin distribution are not yet observable, due to later myelination of smaller caliber axons, like those found in the optic nerve (Hildebrand et al., 1993). Because total heterochromatin to nuclear area ratios were not changed in oligodendrocyte nucleus, the data suggest that levels of euchromatin were not increased. Nikolova et al. (2004) suggested that in the absence of *LMNA*, gene expression is altered due to a disruption of heterochromatin architecture, based on the rationale that gene silencing can be achieved by localization of a gene to heterochromatin (Francastel et al., 1999), however they did not postulate as to whether

expression is increased or decreased. This could indicate that myelin gene expression is altered in the oligodendrocyte nucleus of *LMNA* deficient mice, due to the disruption of peripheral heterochromatin.

### ***LMNA* plays a temporal role in spinal cord myelination**

With the reduction in peripheral heterochromatin observed in oligodendrocytes of the corpus callosum and spinal cord, it was proposed that myelination would be increased in the absence of A type lamins. Using *in situ* hybridization, Nielsen et al. (2002) observed that the myelin specific gene encoding proteolipid protein (*PLP*) preferentially localized to the nuclear periphery. *PLP* is upregulated during differentiation from immature oligodendrocyte to mature myelinating oligodendrocyte (Dubois-Dalcq et al., 1986). Because of this, it was of interest to study if reduction in peripheral heterochromatin lead to increased myelination; however, this result was not observed. No effect on myelin thickness was observed in either the spinal cord or corpus callosum at PND 21. This is potentially due to the timeline of myelination in the murine CNS. Myelination begins in the spinal cord, and continues in a rostral to caudal gradient, and is mostly complete in the mouse by PND 60 (Foran and Peterson, 1992). It is possible that no difference in myelin thickness between the WT and *LMNA* KO was observed at PND 21, because the myelination process was ongoing and the postnatal timeline of the onset of *LMNA* expression.

Thinner myelin was observed in the spinal cord of PND 35 *LMNA* deficient mice, but not in the corpus callosum. This indicates A type lamins may play a role in myelination in a region specific manner, or that the effect is not seen in the corpus callosum as early as PND 35. Because peripheral heterochromatin architecture is affected by the absence of A type lamins in PND 35

corpus callosum oligodendrocytes, it could be hypothesized that the effect of *LMNA* on corpus callosum myelination may have an impact at a time point later than those studied, as myelination in the corpus callosum occurs later than in the spinal cord, with peak myelination continuing to PND 45 (Sturrock, 1980). If possible, studying a time point after peak myelination, ideally when the majority of myelination is completed at PND 60 (Baumann and Pham-Dihn, 2001), would elucidate whether or not the effect of A type lamins on myelin thickness is region specific.. To address how ablation of A type lamins results in thinner myelin, it would be of interest to study the effect of *LMNA* on *PLP* and other myelin gene transcription through q-RT-PCR. From the results obtained, we propose that the alteration in heterochromatin organization in the oligodendrocyte nucleus potentially results in a reduction in myelin gene expression, impacting the thickness of the myelin sheath in the spinal cord of mice.

### ***LMNA* does not impact oligodendrocyte maturity**

As oligodendrocytes mature, their cytoplasm area is reduced and the nuclei become more heterochromatic (Mori and Leblond, 1970). Immature oligodendrocytes do not yet form myelin sheaths (Pfeiffer et al., 1993). Because heterochromatin architecture is altered in spinal cord and corpus callosum oligodendrocytes and myelin is thinner in the spinal cord in the absence of A type lamins at PND 35, it was of interest to determine if *LMNA* has an impact on oligodendrocyte maturity. To study this, ratios of oligodendrocyte nuclear area to cytoplasm area were measured and compared. No difference in oligodendrocyte nuclear area to cytoplasm ratios was observed between WT and *LMNA* KO in either PND 21 or PND 35 mice in the corpus

callosum, spinal cord, or optic nerve. Therefore, the data indicate that oligodendrocyte maturity is not impacted in the absence of A type lamins. It is important to realize that this approach for analyzing oligodendrocyte state of maturation provides only a gross assessment and more subtle differences in maturation states would not be observed by this method. To further test oligodendrocyte maturity, western blots could be conducted looking at markers of mature myelinating oligodendrocytes like MBP and MAG in the absence of *LMNA*.

### **Future directions**

The purpose of this study was to identify if *LMNA* was a potential therapeutic target for altering myelination, which could be used to facilitate myelin repair or replacement in demyelinating diseases such as Multiple Sclerosis. Ablation of *LMNA* resulted in a decrease in peripherally located heterochromatin, but not total heterochromatin, and thinner myelin sheaths temporally and in a potentially region specific manner. It would be interesting to determine if A type lamins impact myelin gene expression, using q-RT-PCR, and to see how levels of myelin related proteins are impacted through western blot studies. Additionally, if overexpression of *LMNA* results in upregulation of myelin genes, *LMNA* may make for a therapeutic target for MS treatment.

Because *LMNA* total knockout mice typically do not survive past 4-6 weeks of age, using an oligodendrocyte specific promoter to create a conditional knockout would allow for further studies to determine specific effects of A type lamins on oligodendrocytes at later time points. It is presumed that the reduced life span of the total *LMNA* KO results from compromised gene

regulation in cells other than oligodendrocytes. In collaboration with the laboratory of Dr. Casaccia, our laboratory has begun preliminary studies on two *LMNA* conditional KO mice, an inducible PLP-cre estrogen receptor (ER) KO and a CNP-cre KO. These mice have a longer life span, and allow us to see the oligodendrocyte specific effects of the absence of A type lamins. The *PLP* promoter drives expression in cell types other than oligodendrocytes during embryonic and early postnatal development (Michalski et al., 2011). However, to avoid this confounding factor, tamoxifen injections in this preliminary study are not performed until the mice are 8 weeks of age. Completing the electron microscopy analyses presented in this study with these oligodendrocyte specific conditional knockouts would clarify whether the observed effects of *LMNA* are truly region specific, or if they are dependent upon the timeline of postnatal development.

### **Concluding remarks**

The observations made in this thesis represent novel findings for the role of A type lamins. While expressed in nearly all cell types postnatally, I show that *LMNA* plays roles specific to oligodendrocytes and myelination, in a potentially region specific manner. These results provide an initial understanding of the role that A type lamins play with regard to CNS myelination, and serve as a foundation for further studies to elucidate mechanisms of *LMNA* on oligodendrocyte gene expression, and provide an epigenetic target for impacting myelin gene expression.

## LITERATURE CITED

- Abdelhak, A., Weber, M.S., and Tumani, H. (2017). Primary Progressive Multiple Sclerosis: Putting Together the Puzzle. *Front Neurol* 8, 234.
- Adam, S.A., and Goldman, R.D. (2012). Insights into the differences between the A- and B-type nuclear lamins. *Adv Biol Regul* 52, 108–113.
- Andrés, V., and González, J.M. (2009). Role of A-type lamins in signaling, transcription, and chromatin organization. *J. Cell Biol.* 187, 945–957.
- Auricchio, F., Scavone, C., Cimmaruta, D., Di Mauro, G., Capuano, A., Sportiello, L., and Rafaniello, C. (2017). Drugs approved for the treatment of multiple sclerosis: review of their safety profile. *Expert Opin Drug Saf* 16, 1359–1371.
- Baecher-Allan, C., Kaskow, B.J., and Weiner, H.L. (2018). Multiple Sclerosis: Mechanisms and Immunotherapy. *Neuron* 97, 742–768.
- Barateau, A., Vadrot, N., Vicart, P., Ferreiro, A., Mayer, M., Héron, D., Vigouroux, C., and Buendia, B. (2017). A Novel Lamin A Mutant Responsible for Congenital Muscular Dystrophy Causes Distinct Abnormalities of the Cell Nucleus. *PLoS ONE* 12, e0169189.
- Bártová, E., Krejčí, J., Harnicarová, A., Galiová, G., and Kozubek, S. (2008). Histone modifications and nuclear architecture: a review. *J. Histochem. Cytochem.* 56, 711–721.
- Baumann, N., and Pham-Dinh, D. (2001). Biology of oligodendrocyte and myelin in the mammalian central nervous system. *Physiol. Rev.* 81, 871–927.
- Belmont, A.S., Zhai, Y., and Thilenius, A. (1993). Lamin B distribution and association with peripheral chromatin revealed by optical sectioning and electron microscopy tomography. *J. Cell Biol.* 123, 1671–1685.

- Benjamins, J.A., and Morell, P. (1978). Proteins of myelin and their metabolism. *Neurochem. Res.* *3*, 137–174.
- Berry, M., Ibrahim, M., Carlile, J., Ruge, F., Duncan, A., and Butt, A.M. (1995). Axon-glia relationships in the anterior medullary velum of the adult rat. *J. Neurocytol.* *24*, 965–983.
- Biamonti, G., Giacca, M., Perini, G., Contreas, G., Zentilin, L., Weighardt, F., Guerra, M., Della Valle, G., Saccone, S., and Riva, S. (1992). The gene for a novel human lamin maps at a highly transcribed locus of chromosome 19 which replicates at the onset of S-phase. *Mol. Cell. Biol.* *12*, 3499–3506.
- Bjartmar, C., Hildebrand, C., and Loinder, K. (1994). Morphological heterogeneity of rat oligodendrocytes: electron microscopic studies on serial sections. *Glia* *11*, 235–244.
- Brady, S., Siegel, G., Albers, R.W., Price, D., and Brady, S. (2005). *Basic Neurochemistry: Molecular, Cellular and Medical Aspects* (Burlington, UNITED STATES: Elsevier Science & Technology).
- Braunstein, M., Rose, A.B., Holmes, S.G., Allis, C.D., and Broach, J.R. (1993). Transcriptional silencing in yeast is associated with reduced nucleosome acetylation. *Genes Dev.* *7*, 592–604.
- Braunstein, M., Sobel, R.E., Allis, C.D., Turner, B.M., and Broach, J.R. (1996). Efficient transcriptional silencing in *Saccharomyces cerevisiae* requires a heterochromatin histone acetylation pattern. *Mol. Cell. Biol.* *16*, 4349–4356.
- Brück, W., and Stadelmann, C. (2003). Inflammation and degeneration in multiple sclerosis. *Neurol. Sci.* *24 Suppl 5*, S265-267.
- Butt, A.M., Colquhoun, K., Tutton, M., and Berry, M. (1994). Three-dimensional morphology of astrocytes and oligodendrocytes in the intact mouse optic nerve. *J. Neurocytol.* *23*, 469–485.

- Butt, A.M., Ibrahim, M., Ruge, F.M., and Berry, M. (1995). Biochemical subtypes of oligodendrocyte in the anterior medullary velum of the rat as revealed by the monoclonal antibody Rip. *Glia* 14, 185–197.
- Butt, A.M., Ibrahim, M., and Berry, M. (1997). The relationship between developing oligodendrocyte units and maturing axons during myelinogenesis in the anterior medullary velum of neonatal rats. *J. Neurocytol.* 26, 327–338.
- Buttermore, E.D., Thaxton, C.L., and Bhat, M.A. (2013). Organization and maintenance of molecular domains in myelinated axons. *J. Neurosci. Res.* 91, 603–622.
- Campagnoni, A.T., and Macklin, W.B. (1988). Cellular and molecular aspects of myelin protein gene expression. *Mol. Neurobiol.* 2, 41–89.
- Cockell, M., and Gasser, S.M. (1999). Nuclear compartments and gene regulation. *Curr. Opin. Genet. Dev.* 9, 199–205.
- Compston, C., and Compston, A. (2008). Multiple sclerosis. *The Lancet* 372, 1502–1517.
- Copray, S., Huynh, J.L., Sher, F., Casaccia-Bonnel, P., and Boddeke, E. (2009). Epigenetic mechanisms facilitating oligodendrocyte development, maturation, and aging. *Glia* 57, 1579–1587.
- Dangata, Y.Y., Findlater, G.S., and Kaufman, M.H. (1996a). Postnatal development of the optic nerve in (C57BL x CBA)F1 hybrid mice: general changes in morphometric parameters. *J. Anat.* 189 ( Pt 1), 117–125.
- Dangata, Y.Y., Findlater, G.S., and Kaufman, M.H. (1996b). Postnatal development of the optic nerve in (C57BL x CBA)F1 hybrid mice: general changes in morphometric parameters. *J. Anat.* 189 ( Pt 1), 117–125.
- Davies, J.E. (2007). The pharmacological basis of therapeutics. *Occup Environ Med* 64, e2.

- Davies, B.S., Coffinier, C., Yang, S.H., Barnes, R.H., Jung, H.-J., Young, S.G., and Fong, L.G. (2011). Investigating the purpose of prelamin A processing. *Nucleus* 2, 4–9.
- Deber, C.M., and Reynolds, S.J. (1991). Central nervous system myelin: structure, function, and pathology. *Clin. Biochem.* 24, 113–134.
- Dendrou, C.A., Fugger, L., and Friese, M.A. (2015). Immunopathology of multiple sclerosis. *Nat. Rev. Immunol.* 15, 545–558.
- Dorner, D., Gotzmann, J., and Foisner, R. (2007). Nucleoplasmic lamins and their interaction partners, LAP2alpha, Rb, and BAF, in transcriptional regulation. *FEBS J.* 274, 1362–1373.
- Dubois-Dalcq, M., Behar, T., Hudson, L., and Lazzarini, R.A. (1986). Emergence of three myelin proteins in oligodendrocytes cultured without neurons. *J. Cell Biol.* 102, 384–392.
- Eng, L.F., Chao, F.C., Gerstl, B., Pratt, D., and Tavaststjerna, M.G. (1968). The maturation of human white matter myelin. Fractionation of the myelin membrane proteins. *Biochemistry* 7, 4455–4465.
- Fawcett, D.W. (1966). On the occurrence of a fibrous lamina on the inner aspect of the nuclear envelope in certain cells of vertebrates. *Am. J. Anat.* 119, 129–145.
- Felsenfeld, G., and Groudine, M. (2003). Controlling the double helix. *Nature* 421, 448–453.
- Fernandez, A.F., Assenov, Y., Martin-Subero, J.I., Balint, B., Siebert, R., Taniguchi, H., Yamamoto, H., Hidalgo, M., Tan, A.-C., Galm, O., et al. (2012). A DNA methylation fingerprint of 1628 human samples. *Genome Res.* 22, 407–419.
- Foran, D.R., and Peterson, A.C. (1992a). Myelin acquisition in the central nervous system of the mouse revealed by an MBP-Lac Z transgene. *J. Neurosci.* 12, 4890–4897.

- Foran, D.R., and Peterson, A.C. (1992b). Myelin acquisition in the central nervous system of the mouse revealed by an MBP-Lac Z transgene. *J. Neurosci.* *12*, 4890–4897.
- Francastel, C., Walters, M.C., Groudine, M., and Martin, D.I. (1999). A functional enhancer suppresses silencing of a transgene and prevents its localization close to centromeric heterochromatin. *Cell* *99*, 259–269.
- Frohman, E.M., Havrdova, E., Lublin, F., Barkhof, F., Achiron, A., Sharief, M.K., Stuve, O., Racke, M.K., Steinman, L., Weiner, H., et al. (2006). Most patients with multiple sclerosis or a clinically isolated demyelinating syndrome should be treated at the time of diagnosis. *Arch. Neurol.* *63*, 614–619.
- Gaesser, J.M., and Fyffe-Maricich, S.L. (2016). Intracellular signaling pathway regulation of myelination and remyelination in the CNS. *Exp. Neurol.* *283*, 501–511.
- Galiová, G., Bártová, E., Raska, I., Krejčí, J., and Kozubek, S. (2008). Chromatin changes induced by lamin A/C deficiency and the histone deacetylase inhibitor trichostatin A. *Eur. J. Cell Biol.* *87*, 291–303.
- Gotzmann, J., and Foisner, R. (2006). A-type lamin complexes and regenerative potential: a step towards understanding laminopathic diseases? *Histochem. Cell Biol.* *125*, 33–41.
- Gregoret, I.V., Lee, Y.-M., and Goodson, H.V. (2004). Molecular evolution of the histone deacetylase family: functional implications of phylogenetic analysis. *J. Mol. Biol.* *338*, 17–31.
- Harr, J.C., Luperchio, T.R., Wong, X., Cohen, E., Wheelan, S.J., and Reddy, K.L. (2015). Directed targeting of chromatin to the nuclear lamina is mediated by chromatin state and A-type lamins. *J. Cell Biol.* *208*, 33–52.
- Hartung, H.-P., Aktas, O., Menge, T., and Kieseier, B.C. (2014). Chapter 1 - Immune regulation of multiple sclerosis. In *Handbook of Clinical Neurology*, D.S. Goodin, ed. (Elsevier), pp. 3–14.

- Hemmer, B., Kerschensteiner, M., and Korn, T. (2015). Role of the innate and adaptive immune responses in the course of multiple sclerosis. *Lancet Neurol* *14*, 406–419.
- Hernandez, M., and Casaccia, P. (2015). Interplay between transcriptional control and chromatin regulation in the oligodendrocyte lineage. *Glia* *63*, 1357–1375.
- Hildebrand, C., Remahl, S., Persson, H., and Bjartmar, C. (1993). Myelinated nerve fibres in the CNS. *Prog. Neurobiol.* *40*, 319–384.
- Hille, H., and Hille, B. *Ionic channels of excitable membranes*. Sunderland, Mass.: Sinauer Associates. xviii, 814.
- Hodgkin, A.L., and Huxley, A.F. (1952). A quantitative description of membrane current and its application to conduction and excitation in nerve. *J. Physiol. (Lond.)* *117*, 500–544.
- Holtz, D., Tanaka, R.A., Hartwig, J., and McKeon, F. (1989). The CaaX motif of lamin A functions in conjunction with the nuclear localization signal to target assembly to the nuclear envelope. *Cell* *59*, 969–977.
- Hutchison, C.J. and Worman, H.J. (2004). A-type lamins: guardians of the soma? *Nat Cell Biol.* *6*, 1062-1067
- Imai, S., Nishibayashi, S., Takao, K., Tomifuji, M., Fujino, T., Hasegawa, M., and Takano, T. (1997). Dissociation of Oct-1 from the nuclear peripheral structure induces the cellular aging-associated collagenase gene expression. *Mol. Biol. Cell* *8*, 2407–2419.
- Jung, H.-J., Lee, J.M., Yang, S.H., Young, S.G., and Fong, L.G. (2013). Nuclear lamins in the brain - new insights into function and regulation. *Mol. Neurobiol.* *47*, 290–301.
- Kremer, I.E.H., Evers, S.M.A.A., Jongen, P.J., van der Weijden, T., van de Kolk, I., and Hilgsmann, M. (2016). Identification and Prioritization of Important Attributes of Disease-Modifying Drugs in Decision Making among Patients with Multiple Sclerosis: A Nominal Group Technique and Best-Worst Scaling. *PLoS ONE* *11*, e0164862.

- Kuhlmann, T., Miron, V., Cui, Q., Cuo, Q., Wegner, C., Antel, J., and Brück, W. (2008). Differentiation block of oligodendroglial progenitor cells as a cause for remyelination failure in chronic multiple sclerosis. *Brain* 131, 1749–1758.
- Kutzelnigg, A., and Lassmann, H. (2014). Chapter 2 - Pathology of multiple sclerosis and related inflammatory demyelinating diseases. In *Handbook of Clinical Neurology*, D.S. Goodin, ed. (Elsevier), pp. 15–58.
- Lin, F., and Worman, H.J. (1993). Structural organization of the human gene encoding nuclear lamin A and nuclear lamin C. *J. Biol. Chem.* 268, 16321–16326.
- Lin, F. and Worman, H.J. (1995). Structural organization of the human gene (LMNB1) encoding nuclear lamin B1. *Genomics.* 27, 230-236.
- Liu, J., and Casaccia, P. (2010). Epigenetic regulation of oligodendrocyte identity. *Trends Neurosci.* 33, 193–201.
- Liu, J., Dietz, K., DeLoyht, J.M., Pedre, X., Kelkar, D., Kaur, J., Vialou, V., Lobo, M.K., Dietz, D.M., Nestler, E.J., et al. (2012). Impaired adult myelination in the prefrontal cortex of socially isolated mice. *Nat. Neurosci.* 15, 1621–1623.
- Liu, J., Moyon, S., Hernandez, M., and Casaccia, P. (2016). Epigenetic control of oligodendrocyte development: adding new players to old keepers. *Curr. Opin. Neurobiol.* 39, 133–138.
- Ma, V.Y., Chan, L., and Carruthers, K.J. (2014). Incidence, prevalence, costs, and impact on disability of common conditions requiring rehabilitation in the United States: stroke, spinal cord injury, traumatic brain injury, multiple sclerosis, osteoarthritis, rheumatoid arthritis, limb loss, and back pain. *Arch Phys Med Rehabil* 95, 986-995.e1.
- Marcus, J., Honigbaum, S., Shroff, S., Honke, K., Rosenbluth, J., and Dupree, J.L. (2006). Sulfatide is essential for the maintenance of CNS myelin and axon structure. *Glia* 53, 372–381.

- McGinty, R.K., and Tan, S. (2014). Histone, Nucleosome, and Chromatin Structure. In *Fundamentals of Chromatin*, (Springer, New York, NY), pp. 1–28.
- Menn, B., Garcia-Verdugo, J.M., Yaschine, C., Gonzalez-Perez, O., Rowitch, D., and Alvarez-Buylla, A. (2006). Origin of oligodendrocytes in the subventricular zone of the adult brain. *J. Neurosci.* *26*, 7907–7918.
- Meuleman, W., Peric-Hupkes, D., Kind, J., Beaudry, J.-B., Pagie, L., Kellis, M., Reinders, M., Wessels, L., and van Steensel, B. (2013). Constitutive nuclear lamina-genome interactions are highly conserved and associated with A/T-rich sequence. *Genome Res.* *23*, 270–280.
- Michalski, J.-P., Anderson, C., Beauvais, A., De Repentigny, Y., and Kothary, R. (2011). The proteolipid protein promoter drives expression outside of the oligodendrocyte lineage during embryonic and early postnatal development. *PLoS ONE* *6*, e19772.
- Moir, R.D., Montag-Lowy, M., and Goldman, R.D. (1994). Dynamic properties of nuclear lamins: lamin B is associated with sites of DNA replication. *J. Cell Biol.* *125*, 1201–1212.
- Mori, S., and Leblond, C.P. (1970). Electron microscopic identification of three classes of oligodendrocytes and a preliminary study of their proliferative activity in the corpus callosum of young rats. *J. Comp. Neurol.* *139*, 1–28.
- Murtie, J.C., Macklin, W.B., and Corfas, G. (2007). Morphometric analysis of oligodendrocytes in the adult mouse frontal cortex. *J. Neurosci. Res.* *85*, 2080–2086.
- Nielsen, J.A., Hudson, L.D., and Armstrong, R.C. (2002). Nuclear organization in differentiating oligodendrocytes. *J. Cell. Sci.* *115*, 4071–4079.
- Nikolova, V., Leimena, C., McMahon, A.C., Tan, J.C., Chandar, S., Jogia, D., Kesteven, S.H., Michalicek, J., Otway, R., Verheyen, F., et al. (2004). Defects in nuclear structure and function promote dilated cardiomyopathy in lamin A/C-deficient mice. *J. Clin. Invest.* *113*, 357–369.

- Ozawa, K., Suchanek, G., Breitschopf, H., Brück, W., Budka, H., Jellinger, K., and Lassmann, H. (1994). Patterns of oligodendroglia pathology in multiple sclerosis. *Brain* 117 ( Pt 6), 1311–1322.
- Padiath, Q.S., Saigoh, K., Schiffmann, R., Asahara, H., Yamada, T., Koeppen, A., Hogan, K., Ptacek, L.J., and Fu, Y.H. (2006). Lamin B1 duplications cause autosomal dominant leukodystrophy. *Nature Genetics*. 38, 1114-1123
- Padiath, Q.S. (2016). Lamin B1 mediated demyelination: Linking Lamins, Lipids and Leukodystrophies. *Nucleus* 7, 547–553.
- Patrikios, P., Stadelmann, C., Kutzelnigg, A., Rauschka, H., Schmidbauer, M., Laursen, H., Sorensen, P.S., Brück, W., Lucchinetti, C., and Lassmann, H. (2006). Remyelination is extensive in a subset of multiple sclerosis patients. *Brain* 129, 3165–3172.
- Paz Soldán, M.M., and Pirko, I. (2012). Biogenesis and significance of central nervous system myelin. *Semin Neurol* 32, 9–14.
- Peterson, J.W., Bö, L., Mörk, S., Chang, A., and Trapp, B.D. (2001). Transected neurites, apoptotic neurons, and reduced inflammation in cortical multiple sclerosis lesions. *Ann. Neurol.* 50, 389–400.
- Pfeiffer, S.E., Warrington, A.E., and Bansal, R. (1993). The oligodendrocyte and its many cellular processes. *Trends Cell Biol.* 3, 191–197.
- Politz, J.C.R., Scalzo, D., and Groudine, M. (2013). Something silent this way forms: the functional organization of the repressive nuclear compartment. *Annu. Rev. Cell Dev. Biol.* 29, 241–270.
- Prineas, J.W., Barnard, R.O., Revesz, T., Kwon, E.E., Sharer, L., and Cho, E.S. (1993). Multiple sclerosis. Pathology of recurrent lesions. *Brain* 116 ( Pt 3), 681–693.

- Purves, P., and Purves, D. (2012). *Neuroscience*.
- Remahl, S., and Hildebrand, C. (1990). Relations between axons and oligodendroglial cells during initial myelination. II. The individual axon. *J. Neurocytol.* *19*, 883–898.
- Richardson, W.D., Kessaris, N., and Pringle, N. (2006). Oligodendrocyte wars. *Nat. Rev. Neurosci.* *7*, 11–18.
- Röber, R.A., Weber, K., and Osborn, M. (1989). Differential timing of nuclear lamin A/C expression in the various organs of the mouse embryo and the young animal: a developmental study. *Development* *105*, 365–378.
- Shroff, S.M., Pomicter, A.D., Chow, W.N., Fox, M.A., Colello, R.J., Henderson, S.C., and Dupree, J.L. (2009). Adult CST-null mice maintain an increased number of oligodendrocytes. *J. Neurosci. Res.* *87*, 3403–3414.
- Smith, A.L., Cohen, J.A., and Hua, L.H. (2017a). Therapeutic Targets for Multiple Sclerosis: Current Treatment Goals and Future Directions. *Neurotherapeutics* *14*, 952–960.
- Smith, A.L., Cohen, J.A., and Hua, L.H. (2017b). Therapeutic Targets for Multiple Sclerosis: Current Treatment Goals and Future Directions. *Neurotherapeutics* *14*, 952–960.
- Snaidero, N., and Simons, M. (2014). Myelination at a glance. *J. Cell. Sci.* *127*, 2999–3004.
- Stangel, M., Kuhlmann, T., Matthews, P.M., and Kilpatrick, T.J. (2017). Achievements and obstacles of remyelinating therapies in multiple sclerosis. *Nat Rev Neurol* *13*, 742–754.
- van Steensel, B., and Belmont, A.S. (2017). Lamina-Associated Domains: Links with Chromosome Architecture, Heterochromatin, and Gene Repression. *Cell* *169*, 780–791.
- Sturrock, R.R. (1980). Myelination of the mouse corpus callosum. *Neuropathol. Appl. Neurobiol.* *6*, 415–420.

- Sullivan, T., Escalante-Alcalde, D., Bhatt, H., Anver, M., Bhat, N., Nagashima, K., Stewart, C.L., and Burke, B. (1999). Loss of A-type lamin expression compromises nuclear envelope integrity leading to muscular dystrophy. *J. Cell Biol.* *147*, 913–920.
- Susuki, K., and Rasband, M.N. (2008). Molecular mechanisms of node of Ranvier formation. *Curr. Opin. Cell Biol.* *20*, 616–623.
- Taniura, H., Glass, C., and Gerace, L. (1995). A chromatin binding site in the tail domain of nuclear lamins that interacts with core histones. *J. Cell Biol.* *131*, 33–44.
- Tremlett, H., Zhao, Y., Rieckmann, P., and Hutchinson, M. (2010). New perspectives in the natural history of multiple sclerosis. *Neurology* *74*, 2004–2015.
- Tsai, M.-Y., Wang, S., Heidinger, J.M., Shumaker, D.K., Adam, S.A., Goldman, R.D., and Zheng, Y. (2006). A mitotic lamin B matrix induced by RanGTP required for spindle assembly. *Science* *311*, 1887–1893.
- Tullman, M.J. (2013). Overview of the epidemiology, diagnosis, and disease progression associated with multiple sclerosis. *Am J Manag Care* *19*, S15-20.
- Verkhatsky, A., and Butt, A.M. (2013). *Glial Physiology and Pathophysiology* (Hoboken, UNITED KINGDOM: John Wiley & Sons, Incorporated).
- Wallrath, L.L., Vitalini, M.W., and Elgin, S.C.R. (2014). Heterochromatin: A Critical Part of the Genome. In *Fundamentals of Chromatin*, (Springer, New York, NY), pp. 529–552.
- Wegner, C., Esiri, M.M., Chance, S.A., Palace, J., and Matthews, P.M. (2006). Neocortical neuronal, synaptic, and glial loss in multiple sclerosis. *Neurology* *67*, 960–967.
- Yáñez-Cuna, J.O., and van Steensel, B. (2017). Genome-nuclear lamina interactions: from cell populations to single cells. *Curr. Opin. Genet. Dev.* *43*, 67–72.

Young, S.G., Jung, H.-J., Coffinier, C., and Fong, L.G. (2012). Understanding the roles of nuclear A- and B-type lamins in brain development. *J. Biol. Chem.* 287, 16103–16110.

Zhang, H., Kieckhafer, J.E., and Cao, K. (2013). Mouse models of laminopathies. *Aging Cell* 12, 2–10.

## VITA

Jacqueline Michelle DeLoyht was born on November 29, 1983 in Richmond, VA. She graduated from Collegiate School in Richmond, VA in 2002. She then received her Bachelor of Science in Biology with a minor in chemistry from Virginia Commonwealth University in 2011.